2001

Metal enrichment of the intergalactic medium in cosmological simulations

A Aguirre

L Hernquist

J Schaye

N Katz
University of Massachusetts - Amherst

DH Weinberg

See next page for additional authors

Recommended Citation

Aguirre, A; Hernquist, L; Schaye, J; Katz, N; Weinberg, DH; and Gardner, J, "Metal enrichment of the intergalactic medium in cosmological simulations" (2001). *ASTROPHYSICAL JOURNAL*. 349.
https://doi.org/10.1086/323370

Accepted by The Astrophysical Journal
Preprint typeset using LaTeX style emulateapj v. 04/03/99

METAL ENRICHMENT OF THE INTERGALACTIC MEDIUM IN COSMOLOGICAL SIMULATIONS

Anthony Aguirre,[a,b] Lars Hernquist,[b] Joop Schaye,[a] Neal Katz,[c] David H. Weinberg,[d] & Jeffrey Gardner[e]

[a]Institute for Advanced Study, School of Natural Sciences, Princeton NJ 08540
[b]Department of Astronomy, Harvard University 60 Garden Street, Cambridge, MA 02138
[c]Department of Astronomy, University of Massachusetts, Amherst, MA 01003
[d]Department of Astronomy, Ohio State University, Columbus, OH 43210
[e]Department of Astronomy, University of Washington, Seattle, WA 98195

Accepted by The Astrophysical Journal

ABSTRACT

Observations have established that the diffuse intergalactic medium (IGM) at $z \sim 3$ is enriched to $\sim 10^{-2.5}$ solar metallicity and that the hot gas in large clusters of galaxies (ICM) is enriched to $1/3-1/2\,Z_\odot$ at $z = 0$. Metals in the IGM may have been removed from galaxies (in which they presumably form) during dynamical encounters between galaxies, by ram-pressure stripping, by supernova-driven winds, or as radiation-pressure driven dust efflux. This study develops a method of investigating the chemical enrichment of the IGM and of galaxies, using already completed cosmological simulations. To these simulations, we add dust and (gaseous) metals assuming instantaneous recycling, and distributing the dust and metals in the gas according to three simple parameterized prescriptions, one for each enrichment mechanism. These prescriptions are formulated to capture the basic ejection physics, and calibrated when possible with empirical data. Our method allows exploration of a large number of models, yet for each model yields a specific (not statistical) realization of the cosmic metal distribution that can be compared in detail to observations. Our results indicate that dynamical removal of metals from $\gtrsim 10^{8.5}\,\mathrm{M}_\odot$ galaxies cannot account for the observed metallicity of low-column density Lyα absorbers, and that dynamical removal from $\gtrsim 10^{10.5}\,\mathrm{M}_\odot$ galaxies cannot account for the ICM metallicities. Dynamical removal also fails to produce a strong enough mass-metallicity relation in galaxies. In contrast, either wind or radiation-pressure ejection of metals from relatively large galaxies can plausibly account for all three sets of observations (though it is unclear whether metals can be distributed uniformly enough in the low-density regions without overly disturbing the IGM, and whether clusters can be enriched quite as much as observed). We investigate in detail how our results change with variations in our assumed parameters, and how results for the different ejection processes compare.

Subject headings: cosmology: theory – intergalactic medium – galaxies: formation, starburst – hydrodynamics

1. INTRODUCTION

In the standard hot big-bang cosmological model, elements of atomic number $Z > 2$ cannot form in appreciable quantities until the first stars form. Thereafter, the universe becomes progressively enriched with heavy elements (metals) as stars release these fusion products in stellar winds or supernova ejecta. Stars only form efficiently in dense gas, almost all of which is bound in galaxies (or protogalaxies at high z) with deep gravitational wells. Despite this, the observed intergalactic medium (IGM) shows substantial metal enrichment at all redshifts and at all densities yet measured, from the lowest-density Lyα absorbers at $z > 3$ with $\gtrsim 1/1000$ solar metallicity, to the hot gas with 1/3-1/2 $Z_\odot$ bound in present-day galaxy clusters. A significant fraction, perhaps even a majority, of cosmic metal appears to lie in the IGM. At very high redshift ($z \gg 5$) population III stars could enrich the IGM to a low level (e.g., Carr, Bond & Arnett 1984; Ostriker & Gnedin 1996; Haiman & Loeb 1997; Tegmark et al. 1997; Abel et al. 1998), but since most cosmic metals presumably form in stars in galaxies, a fundamental question arises as to how these metals escape their progenitor galaxies and spread throughout the IGM.

Efforts to understand the enrichment of the IGM by galactic stars (after any Pop. III epoch) have focused on three mechanisms whereby metals could be removed from a galaxy. First, metal-enriched gas (or stars that later explode as Type Ia supernovae) might be unbound during a merger or tidal interaction with another galaxy, or by the ram pressure of the IGM through which the galaxy moves. We shall combine these processes under the name of 'dynamical removal'. Second, the energy input from supernovae may impart sufficient kinetic and thermal energy to galactic gas for it to escape the gravitational well of the galaxy. We shall denote this process as the 'galactic wind' mechanism. Third, the radiation pressure on dust grains due to stellar light may exceed the gravitational force of the matter, leading (if the dust can decouple from the gas) to an outflow of dust. We will denote this possibility by 'radiation-pressure ejection' or 'dust ejection'.[1] (The ejected dust adds metals to the intergalactic *gas* when it

[1]Dust will, however, also be ejected in dynamical removal or wind ejection along with the gas.

is destroyed by thermal sputtering.)

Investigation of the metal enrichment of the IGM requires not only some understanding of how these mechanisms function in a given galaxy, but also calls for knowledge of the properties, distribution, and evolution of galaxies in a cosmological context. Studies of these matters have generally adopted one of two rather different, yet complementary, approaches: the 'numerical' and the 'semi-analytic' methods.

In the numerical approach, an attempt is made to numerically evolve the state of a single sample of the universe from some set of initial conditions, by solving equations of motion encapsulating the most relevant (gravitational, hydrodynamical, etc.) physics. Among the advantages of this approach are that it captures the incorporated physics very well, and that it generates a specific realization of a possible cosmological volume. On the other hand, the available computing power limits the amount of detailed physics and the dynamic range that can be handled. Also, some physical processes must be 'parameterized', and the large computational time prohibits the investigation of large regions of parameter space. The numerical method has been used by Gnedin (1998) to study the enrichment of the IGM by winds and dynamics and employed by Cen & Ostriker (1999) and Gnedin & Ostriker (1997) to study IGM enrichment by dynamics or other (unspecified) processes. Cluster enrichment by galactic winds has been studied using simulations by Metzler & Evrard (1994; 1997) and Murakami & Babul (1999), and the enrichment of the intracluster medium (ICM) through dynamics has been numerically studied by Abadi, Moore & Bower (1999), by Balsara, Livio & O'Dea (1994), and by Quilis, Moore & Bower (2000).

In the semi-analytic approach, predictions are made on a statistical basis, by layering together a number of prescriptions that are individually derived either from theory or observation. This approach allows the investigation of large regions of parameter space, and employs somewhat more complicated physical prescriptions than the numerical method. On the other hand, the flexibility in the input parameters and physical prescriptions leads to a corresponding range in actual predictions, and it is not always clear which physical processes are accurately captured and which are not; nor is it clear that the parameters chosen to best fit the observations are unique. The semi-analytic method has been used by a number of investigators to address IGM enrichment in greatly varying levels of complexity. Nath & Trentham (1997), Ferrara, Pettini & Shchekinov (2000), and Madau, Ferrara & Rees (2000) have studied IGM enrichment by winds in this way, attempting also to calculate the statistical properties of the metal distribution in the IGM. Cluster enrichment by winds has been studied by Dekel & Silk (1986), Nath & Chiba (1995), and David, Forman & Jones (1990), among others. The dynamical enrichment of clusters has been similarly examined a number of times (e.g., Gunn & Gott 1972; Renzini et al. 1993). In both cases the overall degree of enrichment has been assessed, but not the distribution of the metals. Finally, ejection of dust by radiation pressure has been calculated for individual sample galaxies (Chiao & Wickramasinghe 1972; Ferrara et al. 1990; Shustov & Vibe 1995; Davies et al. 1998; Simonsen & Hannestad 1999), but only rough estimates of the overall ensuing IGM enrichment are offered.

The method used in the present work combines aspects of both approaches. The time-dependent distribution of dark matter, gas and stars is taken from already completed cosmological smoothed-particle hydrodynamics (SPH) simulations computed using the method described by Katz, Weinberg & Hernquist (1996). To the gas and star particles, metals are added using fairly simple prescriptions formulated to capture the basic physics of the various processes that can transport metals from galaxies into the IGM. This method yields a numerical realization of the actual distribution of metals in the IGM (as well as in galaxies), yet uses relatively little computing time so that a large number of models can be tested, and the effects of changing both physical prescriptions and parameters can be explored. This method has a number of limitations that will be discussed in detail in the following sections, but it can nevertheless yield important insight into metal ejection and distribution unobtainable by either 'purely' numerical computations (using present technology), or semi-analytical methods.

This paper presents an explication and investigation of the method we have developed. We do not attempt to 'fit' a set of observations using our results, but rather make specific assumptions about our input parameters based on independent considerations, and compare the predictions to observations where available. We also investigate directly the variations in predictions resulting from different parameter choices, and address various methodological and numerical considerations. Studies addressing specific astrophysical questions using the method presented here will be published separately (e.g., Aguirre et al. 2001a,b).

We have organized this paper as follows. Section 2 describes our calculation method, with subsections 2.1, 2.2, and 2.3 detailing prescription for dynamical, wind, and radiation pressure ejection of metals, respectively. These sections also describe the parameters used in the calculation and the fiducial values for these parameters (summarized in Tables 1, 2, 3 and 4). In § 3 we review observations of cluster, galaxy, and Lyα forest metallicity with which we will compare our results. Section 4 briefly compares the SPH simulations (to which we apply our method in this paper) to observations. Sections 23, 6 and 7 present and discuss the trials we have run and the results obtained. We summarize our findings and draw general conclusions in § 8.

2. METHOD

The procedure begins with a set of coarsely-spaced (every $10^8 - 10^9$ yr) snapshots from an SPH cosmological simulation, each containing the states of the dark matter, star, and gas particles at a given redshift. We shall index these particles by 'i', and superscript them by particle type as 'd', 's' or 'g' respectively. We will also denote by $t_{\rm c}$ the time of the output being processed, and by $t_{\rm p}$ the time at the previous output.

Beginning with the first output time where stars exist, the procedure for each time step is as follows. For a star particle i, the stellar mass created since the last step is $\Delta m_i^s(t_{\rm c}) \equiv m_i^s(t_{\rm c}) - m_i^s(t_{\rm p})$. This mass was taken from a gas particle also indexed by i, so the first task is to transfer the metals associated with this gas mass from the gas

particle to the star particle:

$$w_i^s(t_c) = w_i^s(t_p) + \Delta m_i^s(t_c) \times [w_i^g(t_p)/m_i^g(t_p)] \quad (1)$$
$$w_i^g(t_c) = w_i^g(t_p) - \Delta m_i^s(t_c) \times [w_i^g(t_p)/m_i^g(t_p)],$$

where w_i is the metal mass of the ith particle.

We next assume that each unit of forming stellar mass instantaneously ejects y_* units of metal mass into the gas, so that the star particle i adds a metal mass of $\Delta m_i^s(t_c) \times y_*$ to the gas particles. The metals are distributed over the gas particles in a manner appropriate to the particular process, as described in the next few sections. After all metal is deposited, the process repeats for the next simulation output time.

2.1. *Prescription 1: Local Metal Distribution*

The first prescription for metal distribution is the simplest. The metal mass $\Delta m_i^s(t_c) \times y_*$ is 'scattered' over the 32 gas particles nearest to the star particle i, weighted by the SPH smoothing kernel $W(r, h)$, where $2h$ is the radius of the sphere (about particle i) containing exactly 32 gas particles, and r is the distance from particle i to the gas particle in question (see Hernquist & Katz 1989). Since stars form in these simulations only in dense, cool regions with a converging flow, this prescription places metals only in bound regions such as galaxies.[2] Thus with this prescription intergalactic metal must leave galaxies by being carried by a gas particle that is dynamically removed from a bound region.

2.2. *Prescription 2: Ejection by Galactic Winds*

Galactic winds can distribute metals 'non-locally', i.e. disperse them into gas far away from where they are formed. The prescription used to model this physical effect is as follows. First, we divide the gas and star particles into bound groups (i.e. galaxies) using the SKID algorithm.[3] At each simulation step, each bound group is considered in turn. As described above, the new metal mass $\Delta m_i^s(t_c) \times y_*$ in each star particle i within the group is computed. A fraction $(1 - Y_{ej})$ of this metal is distributed among the 32 gas particles nearest to star particle i as per prescription 1. The remaining fraction is added to the tally for the new metal in the group, Δw^{grp}:

$$\Delta w^{grp} = y_* \times Y_{ej} \times \sum_{i \in grp} \Delta m_i^s(t_c). \quad (2)$$

We then distribute the metal mass w^{grp} within a radius $h^{wind}(\theta, \phi)$ about the 'center of star formation'

$$\vec{r}_c \equiv \left[\sum_{i \in grp} \vec{x}_i^s \Delta m_i^s \right] / \left[\sum_{i \in grp} \Delta m_i^s \right], \quad (3)$$

where $\vec{x}_i^s$ is the position of star i. This simulates the non-local dispersal of metal into the regions where winds carry and deposit them. The metal is distributed so that within the angular ranges $[\cos\theta, \cos\theta + \Delta_{\cos\theta}]$ and $[\phi, \phi + \Delta_\phi]$, the metal mass within a shell of width dr at radius r is proportional to $W^{grp}(r, h^{wind}(\theta, \phi))dr$; uniform distribution of metals within the angular region thus corresponds to $W^{grp}(r, h^{wind}(\theta, \phi)) = r^2$.

Choosing values of $h^{wind}(\theta, \phi)$, Y_{ej} and $W^{grp}(r, h^{wind})$ for each galaxy requires some understanding of the physics of galactic winds. The idea that galaxies might drive outflowing winds has a fairly long history. Galactic-scale winds, in which supernova bubbles can overlap and drive a coherent wind across the galaxy before they can cool, have been theoretically investigated in dwarf (e.g., Mac Low & Ferrara 1999), elliptical (e.g., David, Forman & Jones 1990; 1991 and references therein), and starburst spiral (e.g., Heckman et al. 2000, hereafter HLSA; Lehnert & Heckman 1996) galaxies. In the last case, such winds can be observed in some detail as high velocity bipolar outflows seen in many starburst galaxies such as M82 (e.g., Lehnert, Heckman & Weaver 1999). Even if the conditions to drive a coherent galactic-scale wind do not exist, winds capable of ejecting matter into the IGM may still develop: a two-phase ISM with a hot phase fed by supernova remnants can lead to a stochastic 'steady-state' in which some fraction of matter has high enough kinetic energy – perhaps aided by cosmic-ray pressure (e.g., Breitschwerdt et al. 1991) – to escape the galaxy (especially near concentrations of supernovae). Winds of this sort have been investigated theoretically by Efstathiou (2000), Ferrara & Tolstoy (2000), Breitschwerdt & Schmutzler (1999), and Ferrara, Pettini & Shchekinov (2000). Thus we see that winds may be starburst-driven, driven by 'quiescent' star formation, or cosmic ray-driven, and that they may be 'global' or 'local'. These distinctions can readily break down, however: in dwarfs or in galaxies with very rapid star-formation, the local/global distinction breaks down, and at high-z (where star formation is vigorous and mergers common) there is probably no clear line between starbursts and quiescent star formation.

Despite their differences, all of the wind types we have described share some common features:

1. The energy release in supernovae is the ultimate source of the wind energy. Some critical supernova rate is necessary for a galactic-scale wind to form and blow out of the disk.

2. The wind speed may exceed the escape velocity of the progenitor galaxy, but the wind and the swept-up material must stall or become pressure-confined at some radius.

3. It is physically reasonable for the wind's energy to be tied to the star formation rate.

The method used in our investigation is based primarily on observations of galactic-scale 'superwinds' and has been formulated to capture these three key physical features in a simple and general way, so that it can be reasonably applied to galactic winds of all types (with varying degrees of confidence). First, we assume some critical SFR/(area), SFR_{crit}, below which wind development is suppressed. For

[2] If stars form in bound groups with < 32 gas particles, some metals will be placed in particles outside the bound group.

[3] SKID is publicly available at http://www-hpcc.astro.washington.edu/tools. We require also that these groups have at least 4 (gas+star) particles and a minimal overdensity of 50; groups of between 1 and 4 particles are treated as 'ungrouped', but essentially no star formation takes place in these areas.

thermal winds, this should physically correspond to a rate above which supernova remnants can overlap before cooling (David, Forman & Jones 1990; Efstathiou 2000; Heckman, Armus & Miley 1990). This assumption is supported by observations indicating that superwinds in spirals develop when the SFR/unit area (averaged over the disk) reaches a critical value (Martin 1999; Heckman 2000). Since the 'areas' of spiral galaxies are not robustly determined in the simulations, we compute galaxy areas from their masses, using the empirical mass-radius relation[4] of Gavazzi, Pierini & Boselli (1996), who find (area)$\propto M^{0.78}$.

We allow all galaxies to drive winds, with an initial wind velocity $v_{\rm out}$ and mass outflow rate $\dot{m}_{\rm out}$. Guided by observations of starburst-driven superwinds (Heckman et al. 2000; Martin 1999) indicating mass outflow rates similar to the galaxies' SFRs (for a wide range of SFRs), we express $\dot{m}_{\rm out}$ in units of the SFR.[5] Assuming that one supernova forms per $M_{100}100$ $M_\odot$ of star formation and releases $10^{51}E_{51}$ ergs of energy, the outflow rate $\dot{m}\times$ (SFR) (in $M_\odot$/yr) can be related to the fraction χ of the supernova energy that is incorporated into the wind's kinetic energy $\dot{m}v_{\rm out}^2\times$ (SFR), by

$$\chi \simeq 0.75\,\dot{m}_{\rm out}\left(\frac{v_{\rm out}}{600\,{\rm km\,s^{-1}}}\right)^2 E_{51}^{-1}M_{100}, \qquad (4)$$

where $v_{\rm out}$ is the wind velocity.

We use fixed values of $\rm SFR_{crit}$ and χ that are based on the data available for superwinds (see § 2.2.1 below). For $v_{\rm out}$, we assume a uniform distribution of values with mean $v_{\rm out}^{\rm fid}$ and width $\sigma_{\rm out}$. Given χ and $v_{\rm out}$ for a given galaxy, we compute $\dot{m}_{\rm out}$ using Eq. 4. For galaxies with SFR/(area) $<$ $\rm SFR_{crit}$, we attenuate $v_{\rm out}$ by a factor $(\rm SFR/SFR_{crit})^\beta$ and attenuate χ by a factor $(\rm SFR/SFR_{crit})^{2\beta}$. This lowers both the energy of the wind and the energy of the initial shell by a factor $(\rm SFR/SFR_{crit})^{2\beta}$, and therefore suppresses winds in low-SFR galaxies as desired.

We assume that in each direction (θ,ϕ) the wind flows to some maximum radius $h^{\rm wind}(\theta,\phi)$, then joins the dynamics of the ambient gas. This radius, within which the galaxy's metals are distributed, is again determined from the physics of winds. When a bubble of supernova-heated gas forms and begins to expand, several things can stop its growth. First, the ISM of the host galaxy will be swept into a shell which, if massive enough, can confine the wind to the galaxy, as happens in an ordinary single supernova explosion. If the bubble has enough energy, the shell can be blown out of the disk, whereupon it may partially fragment due to the Raleigh-Taylor instability or because of density inhomogeneities in the ambient medium; the hot wind can then stream past the shell, entraining it (and perhaps other portions of the ISM) into a mass-loaded outflow. The process may then repeat.

For each of N_a directions (θ,ϕ), we compute the maximum radius to which the wind could expand by following the dynamics of a 'test' shell of physical radius r about $\vec{r}_c$, with mass $m(r)$ and outward radial velocity $v(r)$. This shell represents the initial wave of matter swept up by the developing wind, and feels four forces: the wind's ram pressure, gravity, the thermal pressure of the ambient gas, and the ram pressure of any infalling ambient gas[6] Under these four forces the shell momentum evolves according to

$$\frac{d}{dt}(mv) = \frac{\dot{m}_{\rm out}}{N_a}(v_w - v) - m\frac{d\bar{\phi}}{dr} - \left(\frac{4\pi}{N_a}\right)r^2\bar{p} + \epsilon_{\rm ent}\left(\frac{4\pi}{N_a}\right)r^2\bar{\rho}\,(\bar{v}_{\rm rad}+Hr)\,(v-\bar{v}_{\rm rad}-Hr), \qquad (5)$$

and the mass evolves as

$$\frac{d}{dt}(m) = \frac{\dot{m}_{\rm out}}{N_a}\left(1-\frac{v}{v_w}\right)+\epsilon_{\rm ent}\left(\frac{4\pi}{N_a}\right)r^2\bar{\rho}\,(v-\bar{v}_{\rm rad}-Hr)\,. \qquad (6)$$

Here, $\bar{\rho}(r)$, $\bar{p}(r)$, $\bar{\phi}(r)$ and $\bar{v}_{\rm rad}(r)$ are the average density, thermal pressure, gravitational potential and outward radial peculiar velocity of the ambient medium at radius r, $v_w(r)$ is the wind velocity, and $H(z)$ is the Hubble constant at redshift z:

$$H^2(z) = H_0^2\left[(1+z)^3\Omega + \Omega_\Lambda + (1+z)^2(1-\Omega-\Omega_\Lambda)\right].$$

The averages are done over all particles within the angular ranges $[\cos\theta, \cos\theta+\Delta_{\cos\theta}]$ and $[\phi,\phi+\Delta_\phi]$ and the radial range[7] $[0.95r, 1.05r]$. The angles are spaced in N_θ segments of $\Delta_{\cos\theta}\equiv 2/N_\theta$ in $\cos\theta$ and $N_\phi = 2N_\theta$ segments of $\Delta_\phi\equiv 2\pi/N_\phi$ in ϕ, giving $N_a = N_\theta N_\phi$ portions of equal solid angle. We choose N_a for each galaxy to be 1/16th of the number of gas+star particles in the galaxy; tests show that this gives a small enough number of angles for the radial integrations to be accurate (see also § 6).

The entrainment parameter $\epsilon_{\rm ent}$ is the fraction of ambient material we assume to be swept up by the wind; a perfectly homogeneous shell expanding into a homogeneous medium would give $\epsilon_{\rm ent}=1$, whereas $\epsilon_{\rm ent}\ll 1$ might describe a very clumpy ambient medium with a very small filling factor that the wind can easily stream past (while filling in the 'holes' after passing), or a shell that repeatedly fragments, leaving behind a fraction $(1-\epsilon_{\rm ent})$ of its mass. (Note that we have not included ϵ in the terms accounting for the wind on the shell, as would be appropriate if the shell itself had a small filling factor.)

The wind velocity $v_w(r)$ is $v_{\rm out}$, attenuated by gravity:

$$v_w(r) = \sqrt{(v_{\rm out})^2 - 2[\bar{\phi}(r)-\bar{\phi}(r_0)]}, \qquad (7)$$

where r_0 is the initial radius of the test shell, defined below.

The physical radial velocity of the shell with respect to the ambient gas is $v-\bar{v}_{\rm rad}-Hr$, so evolving (mv) and

[4]The masses derived by Gavazzi et al. from rotation curves will include some dark matter contribution not included in the corresponding simulation galaxy mass. This should not affect large galaxies too much but may be important in dwarfs. See § 2.2.

[5]This mass outflow rate, using the current methodology, does not really determine how much metal leaves the galaxy, merely the 'strength' of the wind.

[6]This purely momentum-based method is similar to that of Theuns, Mo, & Schaye 2001; other studies such as Tegmark, Silk, & Evrard 1993, Nath & Trentham (1997) and Scannepieco & Broadhurst 2001 use slightly different approach in which the shell is driven by thermal (not kinetic) energy so that the internal energy of the 'bubble' must be evolved.

[7]Other prescriptions for the radius to average over could be used, but experimentation shows that the integration is not sensitive to the averaging scheme so we employ this simple one.

m until $v(r) - v_{\rm rad} - Hr < \delta \times Hr$ ($\delta \ll 1$) gives the radius $r_{\rm stall}$ and time $\tau_{\rm stall}$ at which the shell stalls and mixes with the ambient gas (i.e. moves a distance $\delta \times r$ in another Hubble time; we choose $\delta = 0.05$). We set initial conditions for m, v and r by choosing a radius r_0 to include a fixed fraction ξ of the galaxy's mass $M_{\rm gal}$. The initial shell mass is then $m(r_0) = \epsilon_{\rm ent}\xi M_{\rm gal}/N_a$, and $v(r_0) = v^0_{\rm out}$. (The fraction ξ is calibrated to give values of r_0 similar to the radii at which winds from starburst galaxies are observed; see § 2.2.1 below).

The stalling radius must be modified by two effects resulting from our general method, in which we deposit metal generated between times $t_{\rm p}$ and $t_{\rm c}$ in the IGM at time $t_{\rm c}$ rather than at the more appropriate average time $(t_{\rm p} + t_{\rm c})/2 + \tau_{\rm stall}$. First, if $(t_{\rm p} + t_{\rm c})/2 + \tau_{\rm stall}$ exceeds the time $t_{\rm obs}$ at which the results for metal enrichment are desired, we would allow metals to move to erroneously large radii; thus we limit the shell to have $\tau_{\rm stall} < t_{\rm obs} - (t_{\rm p} + t_{\rm c})/2$. Second, if $\tau_{\rm stall} + (t_{\rm p} + t_{\rm c})/2 > t_{\rm c}$, then metal deposited at $t_{\rm c}$ will effectively be artificially carried by the movement of the gas particles between $t_{\rm c}$ and $\tau_{\rm stall} + (t_{\rm p} + t_{\rm c})/2$. For example, if the shell stalls in a region with radial velocity $v_{\rm rad}$ and its metal were deposited at $t_{\rm c}$, then at the appropriate distribution time $\tau_{\rm stall} + (t_{\rm p} + t_{\rm c})/2$ the metal would be in particles at radius (roughly) $r_{\rm stall} + v_{\rm rad}[\tau_{\rm stall} + (t_{\rm p} - t_{\rm c})/2]$, rather than at $r_{\rm stall}$. To compensate for this, after the shell reaches $r_{\rm stall}$ we continue to integrate in radius, but using $dr/dt = -v_{\rm rad}(r)$ for a time $\tau_{\rm stall} + (t_{\rm p} - t_{\rm c})/2$ (or $t_{\rm obs} - t_{\rm c}$ if this is smaller), to reach a final radius $h_{\rm wind}$. Then $h_{\rm wind}$ will be such that metal deposited at $h_{\rm wind}$ will end up at $r_{\rm stall}$ after being carried by the gas particle movement for time $\tau_{\rm stall} + (t_{\rm p} - t_{\rm c})/2$. This assumes that the radial peculiar velocity field in the galaxy's neighborhood changes on a timescale somewhat longer than $\tau_{\rm stall} + (t_{\rm p} - t_{\rm c})/2$. A similar (small) error of the opposite sign arises if $\tau_{\rm stall} + (t_{\rm p} + t_{\rm c})/2 < t_{\rm c}$. In this case, we compensate for this error by integrating $dr/dt = v_{\rm rad}(r)$ after stalling, for the time $(t_{\rm c} - t_{\rm p})/2 - \tau_{\rm stall}$ to obtain $h_{\rm wind}$.

The metal mass is then distributed within the radius $h^{\rm wind} = \min(r_{\rm stall}, r_{\rm max})$, if $r_{\rm stall} > 2r_0$. If $r^{\rm stall} < 2r_0$, the wind has been efficiently confined, and we instead distribute the metal 'locally' as per prescription 1.

The outlined prescription is based on empirical data concerning galactic-scale superwinds driven by starburst nuclei. For other types of winds (cosmic ray driven winds, 'quiescent' winds, 'local' winds, etc.) there is far less useful observational data; most of our understanding of such winds derives from theoretical work (e.g., Breitschwerdt et al. 1991; Efstathiou 2000, Ferrara & Tolstoy 2000; Breitschwerdt & Schmutzler 1999, and Ferrara, Pettini & Shchekinov 2000). Rather than invent a new prescription for these winds (based on the theoretical work), we have chosen to model them with the same prescription as for starburst-driven superwinds, but with different parameters. We shall lump these other types of winds into the category of 'quiescent winds', which will be characterized by a lower critical SFR (so that essentially all galaxies drive winds), but also a lower χ since the winds would not be as efficient.

The general wind prescription captures the essential physics of winds well, and and should provide a good prediction of the dispersal of metals by winds with a given assumed set of physical parameters. Since we do not model the winds in full physical detail, however, a number of methodological details merit attention.

1. Adding metals after the completion of the simulation precludes any self-consistent treatment of the effects of the winds on the gas near the galaxy. This means that we cannot assess the importance of earlier outflows in the escape of later outflows and motivates our approach of assuming a 'steady state' wind running into an undisturbed IGM. Also, we do not treat the interaction of winds from a given galaxy with those from nearby galaxies. Thus galaxies can (unrealistically) pollute wind-driving neighbors, but only at a small level.

2. The method also glosses over the detailed structure of the outflowing wind; we have lumped the details of the wind's interactions with the ambient medium into the parameter $\epsilon_{\rm ent}$, assumed not to vary with radius or among different galaxies.

3. We neglect the effect of the matter within the test shell radius on the wind that drives the shell. This is correct for $\epsilon_{\rm ent} = 1$ (since then there *is* no matter within the shell) and for $\epsilon_{\rm ent} = 0$ (since then the wind passes through the matter). For intermediate values, the wind will have a somewhat lower mass $\dot{m}$ and higher velocity v_w than the mass and velocity $\dot{m}(\epsilon_{\rm ent}), v_w(\epsilon_{\rm ent})$ that it should have had. Fortunately these effects largely cancel out since (in the limit where gravity is unimportant), $\dot{m}(\epsilon_{\rm ent})v_w(\epsilon_{\rm ent}) = \dot{m}v_w$ by momentum conservation.

4. We assume a purely kinetic wind impinging upon the shell at all stages. This leads to the neglect of the pressure inside the shell in Equation 5. It also allows us to disregard shocks and cooling, since the internal energy of the shell does not affect its propagation. We retain the external pressure term so that environments of very high pressure (i.e. clusters) are not treated incorrectly.

5. Although we compute the maximum wind radius with good accuracy, the deposition profile within this radius, $W^{\rm grp}(r, h)$, must simply be assumed. (But we will demonstrate that the details of the assumed form are not too important).

6. Our method assumes that the properties of galaxies driving winds changes on a timescale that is long compared to the outflow time. In particular, we assume that the SFR is constant while the wind propagates. We check this assumption in § 6.

7. The SFRs we use are averaged over the interval between simulation output times (typically $10^8 - 10^9$ yr). Weinberg et al. (2000) find that such averages are a good approximation to the computed 'instantaneous' SFRs. However, the simulations cannot resolve the small (few hundred pc) scale of starburst nuclei, so real starbursts may be shorter and more intense than the smoothly-varying SFR the simulations would suggest, and lead to a larger scatter in

the SFR/area than occurs in the simulated galaxies (see Davé et al. 1999b). This is not a problem for more 'quiescent' winds but complicates the use and choice of a critical wind-driving SFR if winds are assumed to be primarily starburst-driven.

8. Our method concentrates all star formation at a point, from which the wind emanates. This maximizes the effect of the wind and is appropriate in modeling starbursts, but overestimates the wind effectiveness if star formation is distributed over the galaxy. On the other hand, we assume that the wind energy is distributed isotropically. Realistically, winds in their early thermally-dominated phase will be funneled into a bi-conical outflow (e.g., Mac Low & Ferrara 1999) observations show biconical outflows with solid angles of $\sim 0.8\pi - 2.4\pi$ radians at small (few kpc) radii (HLSA; Lehnert & Heckman 1996). Thus realistic winds would have a higher energy per unit solid angle and a more effective outflow in those directions.

9. If $h^{\rm wind}$ is small compared to the size of the galaxy but $r_{\rm stall} > 2r_0$, the given prescription will artificially concentrate metals in the radius $h^{\rm wind}$ about $\vec{r}_c$. This indicates that metallicity gradients in the objects should not be trusted, and that the efficiency of dynamical removal (which cannot easily remove metals from galaxy cores) may be suppressed.

2.2.1. *Fiducial Parameter Values for Wind Ejection*

The key parameters we need to determine are the mean outflow velocity $v_{\rm out}^{\rm fid}$, the width $\sigma_{\rm out}$ of the velocity distribution, the fraction of supernova energy in the wind χ, the critical SFR/kpc^2 (SFR$_{\rm crit}$), the enclosed mass fraction ξ determining the initial shell radius, and the entrainment fraction $\epsilon_{\rm ent}$.

We base these values as much as possible on observations of galaxies with supernova-driven winds, as recently compiled by HLSA and by Martin (1999). HLSA measure both the width $W \sim 300 - 600\,{\rm km\,s^{-1}}$ and velocity offset $v_{\rm out} \sim 100 - 300\,{\rm km\,s^{-1}}$ (from the galaxy's inferred center-of-mass velocity) of NaI absorption lines. Their interpretation of these values is that cool material is being accelerated by a hot outflowing wind. $v_{\rm out}$ is the characteristic velocity of this outflowing material at small radii and $v_{\rm term} \equiv v_{\rm out} + W/2 \sim 600\,{\rm km\,s^{-1}}$ is the inferred 'terminal velocity' to which the dense gas is accelerated, i.e. the velocity where it is roughly comoving with the hot gas (see HLSA). This view is supported by the rough agreement of the inferred $v_{\rm term}$ values with those inferred from X-ray data (HLSA; Martin 1999). ¿From the combined data set of HLSA we take $v_{\rm out}^{\rm fid} = 600\,{\rm km\,s^{-1}}$, $\sigma_{\rm out} = 200\,{\rm km\,s^{-1}}$. Very similar values of $v_{\rm out}$ and W are found for Lyman-break galaxies at $z \sim 3$ (Pettini et al. 2000). Somewhat unexpectedly, according to current data the outflow velocities do *not* seem to be correlated with either the SFR or the mass of the host galaxies (HLSA; Martin 1999; Heckman, private communication). Hence we use a fixed value, though a different prescription may be called for if future observations reveal some dependence on galaxy properties.

In using the observed outflow velocities, we are making an important assumption: a single velocity characterizes the outflowing cool gas and the hotter wind. It is likely, however, that the multiple components of the outflow have rather different velocities.[8] Two-component plasma fits to the X-ray data tend to give temperatures corresponding to velocities that bracket the $v_{\rm term}$ inferred from absorption lines, but the X-ray observations only measure the thermal energy of the gas; numerical simulations suggest that it may have a kinetic energy $\sim 2-3$ times higher, i.e. velocities of $\sim 800 - 1000\,{\rm km\,s^{-1}}$ (HLSA; see also Strickland & Stevens 2000). If this hotter gas contains a mass comparable to the cool material, it may dominate the pressure of the outflowing gas. Another possibility is that the outflowing cool gas may be better characterized by the observed velocity offset $v_{\rm out} \sim 200 - 300\,{\rm km\,s^{-1}}$. This would follow if the absorption occurred in a thin shell that might break up but is inefficiently accelerated by the hotter wind. In this case, the ram pressure of the outflow might be dominated by the high-velocity but low-density wind, or alternatively by the higher-density but lower-velocity entrained clumps. This ambiguity is a significant source of uncertainty, but the results should be bracketed by models with velocities of $\sim 300\,{\rm km\,s^{-1}}$ and $\sim 1000\,{\rm km\,s^{-1}}$, and we will test such values in our calculations.

The mass outflow rate from a wind-producing galaxy can be roughly estimated by measuring the column density of the wind material, then assuming either a thin shell (Pettini et al. 2000; Martin 1999) or a spherical mass-conserving wind (e.g., HLSA). Either way, estimated mass outflow rates are $\sim 1 - 4$ times the galaxy's estimated SFR. Using Equation 4, this can be converted into a fiducial value of $\chi \approx 1$. (This does not mean that we assume supernovae drive winds with perfect efficiency, since probably $E_{51} \neq 1$ or $M_{100} \neq 1$ in Eq. 4; χ is *proportional* to the true wind-driving efficiency, calibrated by the observed velocities and mass outflow rates for winds.) As noted above, for SFR/(area) $<$ SFR$_{\rm crit}$ we attenuate the wind energy by $({\rm SFR/SFR_{crit}})^{2\beta}$. We use $\beta = 2$ as a default, but investigate $\beta = 1, 2, 4, \infty$ to check the dependence on the abruptness of the cutoff.

The entrainment fraction for the winds depends on the clumpiness of the IGM, and on instabilities in the outer shell of an expanding wind. There is currently no good basis – theoretical or observational – for a particular assumption of $\epsilon_{\rm ent}$, so we will try values between 1% and 100% with a fiducial value of 10%.

The critical SFR/area to drive a wind can be roughly addressed using observations. Observational samples of 'normal' star-forming disks versus starbursts indicate that normal disks tend to have SFR/(area) of $0.001 - 0.1\,{\rm M_\odot\,yr^{-1}\,kpc^{-2}}$, whereas starburst regions typically have $0.1 - 1000\,{\rm M_\odot\,yr^{-1}\,kpc^{-2}}$ (Kennicutt 1998). Heckman (2000) finds a similar threshold for starburst-driven superwinds of $0.1\,{\rm M_\odot\,yr^{-1}\,kpc^{-2}}$.[9] We adopt this value as our fiducial SFR$_{\rm crit}$. This choice, as will be discussed in § 6, leads to winds in most (but not all) galaxies at $z > 2$, and about half of the galaxies at $z = 1$. However, as noted above, the simulated galaxies do not attain the *very* high areal SFRs seen in starburst galaxies because

[8] Indeed, as shown in Fig. 7 the wind velocity substantially exceeds the shell velocity.

[9] Martin (1999) finds a much smaller threshold of (few)$\times 10^{-4}\,{\rm M_\odot\,yr^{-1}\,kpc^{-2}}$. The reason for this large disparity is unclear.

TABLE 1
WIND PARAMETERS

Parameter	Description	Default value	Range
$\mathrm{SFR_{crit}}$	critical SFR/(disk area) for thermal wind	$0.1\mathrm{M_\odot/yr/kpc^2}$	0.001-0.2
$v_{\rm out}^{\rm fid}$	outflow velocity at initial radius r_0	600 km/s	300-1000
$\sigma_{\rm out}$	width of outflow velocity distribution	200 km/s	-
χ	'fraction' of supernova energy in wind (c.f. § 2.2)	1.0	0.5-2
$\epsilon_{\rm ent}$	fraction of ambient material entrained in wind	0.1	0.01-1
ξ	fraction of galaxy mass enclosed within initial radius	0.1	0.05-0.2
$Y_{\rm ej}$	fraction of metals distributed non-locally	1.0	0.5-1.0
$f_{\rm dust}^{\rm ej}$	portion of ejected metals in dust	0.5	0.0-0.5
α	$W^{\rm grp} \propto (r/h)^\alpha$	3	1-4
β	Wind and initial shell energy attenuated by $(\mathrm{SFR/SFR_{crit}})^{2\beta}$.	2	$1, 2, 4, \infty$

we average the SFR over $\gtrsim 10^8\,\mathrm{yr}$ (longer than a typical starburst 'event'), and because the simulations cannot resolve the scale of a typical starburst nucleus. Starbursts that *should* occur in simulated galaxies are therefore washed out in both time and space when we compute our areal SFRs. Thus we are essentially assuming that simulated galaxies exceeding the critical SFR would contain the same sorts of starburst regions as observed galaxies, if only such regions could be resolved. We also investigate 'quiescent' models in which we set a smaller SFR/(area) of $0.001\,\mathrm{M_\odot\,yr^{-1}\,kpc^{-2}}$ so that essentially all galaxies in the simulation drive weak winds.

We start the shells at a radius enclosing a fraction ξ of the galaxy's baryonic mass, and choose ξ so that the initial radii obtained are comparable in scale to the areas observed in the studies upon which we base the wind mass outflow rates and initial velocities. These observed regions are typically 10-100 $\mathrm{kpc^2}$; taking $\xi \sim 0.1$ (our fiducial value) gives $r_0 \sim 1 - 100\,\mathrm{kpc}$ at $z = 0$ for simulation galaxies with circular velocities similar to those of the observed galaxies. We check the importance of ξ in § 6.

Finally, we must choose a form for the distribution function $W(r, h)$. The final distribution of the wind material should presumably be 'piled up' where it is stopped by the IGM (or gravity), as in the bow shocks often observed at the end of jets. But any more detailed assumption of $W(r, h)$ seems difficult to justify. For simplicity and generality, we assume $W(r, h) \propto (r/h)^\alpha$, for $1 \leq \alpha \leq 4$ (with a default of $\alpha = 3$), which should span a range of reasonable cases.

2.3. *Prescription 3: Radiation Pressure Ejection*

For bright galaxies, the outward radiation pressure felt by a dust grain in the interstellar medium (ISM) can exceed the inward gravitational pull, suggesting the possibility that dust grains can be expelled from galactic disks into halos or even into the IGM (see Chiao & Wickramasinghe 1972; Ferrara et al. 1990; Shustov & Vibe 1995; Davies et al. 1998; Simonsen & Hannestad 1999). For a spherical model galaxy with a radially increasing mass/luminosity ratio M/L, this outward efflux would inevitably occur within some critical radius where the radiation pressure and gravitational forces on the grain balance.

In our prescription to model this physical effect, we distribute dust near its progenitor galaxy in a way that reflects the equilibrium distribution of dust 'levitating' at the force-balance radius. The maximum radius at which dust can be in force equilibrium, $h^{\rm dust}$, depends on the galaxy luminosity (which we compute using spectral synthesis) and on the distribution of mass (given directly by the simulation). The radial density profile of the levitating dust depends mostly on the dust properties, described below in § 2.5. We do not calculate the destruction of grains before they reach this radius, but we do (as described in § 2.5) calculate thermal sputtering of dust after it is deposited.

To implement this prescription numerically, we first divide the gas and star particles into bound groups using the SKID algorithm as in the wind prescription, and determine the center of star formation $\vec{r}_c$ using Eq. 3. Then about this center we determine a radius $h^{\rm dust}$ such that the gravitational force due to the matter within $h^{\rm dust}$ balances the outward radiation pressure due to the group's luminosity L_ν, i.e.

$$\frac{1}{4\pi c h^2} \int d\nu\, L_\nu \kappa_\nu = \frac{G M_{\rm tot}(h)}{h^2}, \tag{8}$$

where $M_{\rm tot}(h)$ is the total group mass within h, L_ν is the group luminosity, κ_ν is the dust cross section/unit mass, and we assume spherical symmetry. Assuming a bolometric luminosity $L_{\rm bol}$ and a radiation-pressure efficiency $Q_{\rm pr}(T)$ (defined as the ratio of κ_ν to geometrical cross section per unit mass, $\pi a^2/(4\pi a^3 \rho/3)$, averaged over a blackbody of a temperature T that reasonably approximates the spectrum of a galaxy), we have

$$\frac{L_{\rm bol}}{M_{\rm tot}(h^{\rm dust})} = \frac{16\pi G c a \rho_{\rm dust}}{3 Q_{\rm pr}}, \tag{9}$$

where a is the grain radius, giving

$$\frac{L_{\rm bol}/L_\odot}{M_{\rm tot}/M_\odot(h^{\rm dust})} = 1.76 \left(\frac{Q_{\rm pr}(T)}{a[\,\mu\mathrm{m}]}\right)^{-1} \left(\frac{\rho_{\rm dust}}{\mathrm{g\,cm^{-3}}}\right). \tag{10}$$

To compute $L_{\rm bol}$, we track the 'effective' age τ_i of each star particle, then take $L_{\rm bol}(\tau)$ (in units of $L_\odot/M_\odot$) for

a stellar population of that age from the stellar synthesis models of Bruzual & Charlot (1993),[10] for an assumed IMF. We then sum this luminosity over all star particles in the group:

$$L_{\rm bol} = \sum_{i \in {\rm grp}} m_i^s L_{\rm bol}(\tau_i). \quad (11)$$

To compute τ for a newly formed star particle, we assume that the SFR is constant between simulation outputs, so that the luminosity of stars formed between time steps $t_{\rm p}$ and $t_{\rm c}$ can be computed as

$$L_{\rm bol}(\tau_{\rm eff}) \equiv \frac{1}{t_{\rm c} - t_{\rm p}} \int_{t_{\rm p}}^{t_{\rm c}} dt\, L_{\rm bol}(t - t_{\rm p}). \quad (12)$$

We then invert $L_{\rm bol}(\tau_{\rm eff})$ to obtain $\tau_{\rm eff}$. When a new stellar mass Δm_i is added to an existing star particle of age $\tau_i(t_{\rm p})$ and mass $m_i(t_{\rm p})$, the new effective age $\tau_i(t_{\rm c})$ will be given by

$$L_{\rm bol}(\tau_i(t_{\rm c})) = \frac{L_{\rm bol}(\tau_{\rm eff})\Delta m_i + L_{\rm bol}(\tau_i(t_{\rm p}) + t_{\rm c} - t_{\rm p}) m_i}{m_i + \Delta m}. \quad (13)$$

As pointed out by Davies et al. (1998), the luminosity calculated using Eq. 11 must be corrected for extinction by dust in the galaxy, because radiation re-emitted in the far-infrared (FIR) provides negligible radiation pressure. Large dust corrections have been deduced for high luminosity local spirals (Wang & Heckman 1996) and starbursts (Heckman et al. 1998), and in high redshift star-forming galaxies (e.g., Calzetti & Heckman 1999; Granato et al. 2000). As there is significant disagreement as to what dust correction is appropriate in any given context, the topic requires some discussion. In both starburst nuclei and in disk galaxies, the dust correction (i.e. the ratio $L_{\rm IR}/L_{\rm UV}$) appears to be correlated with bolometric luminosity. Heckman et al. (1998), however, find that the correlation with metallicity is stronger, so the correlation with luminosity (or mass) may be partially the metallicity correlation combined with a luminosity-metallicity relation. For example, Heckman et al. (1998, Figure 2b) give a metallicity-extinction relation of

$$\log(L_{\rm IR}/L_{\rm UV}) = 1.45 + 1.65 \log(Z/Z_\odot), \quad (14)$$

where Z is the oxygen abundance relative to solar, $L_{\rm UV}$ is luminosity at $0.19\,\mu$m, and $L_{\rm IR}$ is the integrated $\sim 40 - 120\,\mu$m luminosity. Combining this with an (elliptical galaxy) luminosity-metallicity relation

$$\log(Z/Z_\odot) = 0.4 \log(L_B/\,L_\odot) - 4.4 \quad (15)$$

(from Zaritsky, Kennicutt & Huchra 1994), we obtain

$$\log(L_{\rm IR}/L_{\rm UV}) = 0.66 \log(L_B/\,L_\odot) - 5.8, \quad (16)$$

that reproduces the slope of the disk galaxy extinction-luminosity relation

$$\log(L_{\rm IR}/L_{\rm UV}) = (0.5 \pm 0.1) \log(L_B/\,L_\odot) - (3.7 \pm 0.7) \quad (17)$$

of Wang & Heckman (1996) tolerably well, even though Eq. 14 was derived for starbursts, Eq. 15 for ellipticals, and Eq. 17 was derived for spiral galaxies. Neither Eq. 14 nor Eq. 17 can straightforwardly be applied as a dust correction: they relate the FIR flux to the UV ($\approx 0.19\,\mu$m) radiation rather than to the UV-optical-NIR radiation (denoted henceforth by the subscript 'opt') that drives dust. We assume a constant relation between UV and UV-optical-NIR attenuation, given by $C_f \equiv \log(L_{IR}/L_{\rm opt})$.[11] This constant is not 'free', however, as there is the observational constraint that the total integrated (over the cosmic history and all galaxies) UV radiation as observed in the UV/optical/NIR background is comparable to the total far infrared emission in the FIR background radiation. Madau & Pozzetti (2000) find that the energy in these two radiation backgrounds have a ratio of $1/3 \lesssim F_{\rm IR}/F_{\rm opt} \lesssim 2$, with a probable value of ≈ 1. Because Eq. 14 along with a mass-metallicity relation can yield an extinction-mass relation, and because the simulations should by themselves give a mass-metallicity relation, we adopt

$$\log(L_{\rm IR}/L_{\rm opt}) = 1.45 + 1.65 \log(Z/Z_\odot) + C_f \quad (18)$$

as a fiducial dust correction, with C_f set by requiring that the total emitted FIR/UV ratio (an output of the calculations) is near unity. This typically leads to values of $C_f \sim -1$. We also allow for the possibility of a dust correction depending purely on luminosity (from Wang & Heckman 1996):

$$\log(L_{\rm IR}/L_{\rm opt}) = 0.5 \log(L_{\rm bol}) - 4.7 + C_F. \quad (19)$$

Here, we use the galaxy bolometric luminosities $L_{\rm bol}$ in place of Wang & Heckman's $L_{\rm UV} + L_{\rm FIR}$. Finally, we also try a constant dust correction $\log(L_{\rm IR}/L_{\rm opt}) = C_f$, in which case $C_f \sim 0$ from the background density constraint.

The dust-corrected luminosity can be used with Eq. 10 to find $h^{\rm dust}$, the metal mass $\Delta w^{\rm grp}$ is then distributed among the gas particles within the radius $h^{\rm dust}$ with the mass profile $W^{\rm grp}(r, h^{\rm dust})$ as in the wind prescription.

For $W^{\rm grp} = \delta(r - h^{\rm dust})$, the prescription accurately captures the physics of dust of a single grain size being ejected from a spherical region with sufficient gas drag on the dust that the grains do not attain escape velocity. In general, the prescription captures the essential physics of dust ejection fairly well, but nevertheless has a number of important shortcomings:

1. Charged grains can be confined to galaxies by magnetic fields. Dust might escape if magnetic fields have a component perpendicular to the galaxy; winds or Parker instabilities exacerbated by the radiation pressure may enhance such a component (Chiao & Wickramasinghe 1972; Ferrara et al. 1991; Shustov & Vibe 1995). Ferrara et al. (1991) and Davies et al. (1998) have also noted that grains are charged only sporadically. Magnetic fields may also be much weaker at high redshifts if they have been amplified by a dynamo. Determining the effects of

[10] The models are available via anonymous FTP from ftp.noao.edu.

[11] Realistically C_f should be constant only for a fixed effective galaxy temperature; see § 7. Also, since Eq. 14 applies to starburst regions, C_f also absorbs geometrical differences in extinction between starburst regions and the dust corrected region.

magnetic fields would require information about the magnetic structure of galaxies, their halos, and the IGM that is presently unavailable, so we will *assume* in this study that dust escapes magnetic confinement (though we emphasize that it also possible that it does not).

2. After its deposition, dust is coupled to gas (i.e. follows the gas particles). Thus dust distributed in the halo can simply fall back into the galaxy, rather than maintaining its distance from the galaxy.

3. More detailed calculations show that grains often attain a high velocity at small radii, carrying them past $h^{\rm dust}$ and perhaps to 'infinity'. Thus our estimates of the radius to which grains could escape is probably an underestimate, because the grains would inevitably reach that radius with some outward velocity that would carry them past it. However, if the gas drag is high (or if magnetic fields are important), the time to escape the galactic disk could exceed the dust destruction time in that environment. Thus only in certain situations would the dust escape the inner galactic region and 'levitate' in the halo as the prescription describes. See Aguirre et al. (2001b) for some discussion.

4. As in the wind case, the method is only fully consistent if the dust ejection time (i.e. the transport time from the disk into its final equilibrium position) is shorter than the interval between simulation outputs or between the ejection time and the time at which results are desired, and shorter than the timescale over which the galaxy properties change. The errors at late times are unlikely to be important (see §§ 2.2, 6) unless the transport time substantially exceeds the time between ejection and 'observation'. Dust moving with the high velocities (up to $\sim 1000\,{\rm km\,s^{-1}}$) found by Shustov & Vibe (1995) would not encounter this problem but slower-moving dust might.

5. The distribution of metals occurs without regard to the existence of nearby galaxies whose luminosity and gravitation would affect the force balance. Also, as in the wind prescription galaxies can (unrealistically) enrich each other with their metallic outflows, though this is a small effect with the distribution method we employ.

6. We ignore the radiation-related forces on grains due to photodesorption and the photoelectric effect (see Weingartner & Draine 2000). Both of these effects would increase the radial force on the grain by a small factor. Also, we neglect the luminosity due to accretion onto black holes.

7. Galaxies are not spherical, so the spatial distribution of 'levitating' grains will only be approximately spherical if $h^{\rm dust}$ is much larger than the characteristic size of the galaxy.

8. The dust correction we apply is rather uncertain. We have chosen a dust correction to the UV-optical-NIR luminosity based on metallicity, and also tried a luminosity-dependent correction. The metallicity correction is reasonable and in accord with observations, but it neglects the *distribution* of dust within galaxies, the gas fraction, and also the effective temperature of the radiation. At higher redshift, galaxies are probably more compact, have higher gas fractions, and emit more light at short wavelengths where dust attenuation is more effective. All of these effects may increase the importance of dust at high z more than the decrease in metallicity suppresses extinction. But the luminosity-dependent correction we try *is* stronger at high z and can be used as a check on our assumptions.

While our prescription for modeling the ejection of dust could be significantly improved given a better understanding of the dust ejection process and of the correct dust correction, it should give a reasonable estimate of which galaxies could eject dust, and of the ejection radius.

2.3.1. *Fiducial Parameter Values for Dust Ejection*

The key physical parameters in the dust ejection model are the dust absorption efficiency, the dust distribution function $W^{\rm grp}$, the adjustment factor C_f in the dust correction to the galaxy luminosity, and the IMF used in the spectral synthesis.

For the dust absorption efficiency, we adopt the values calculated by Laor & Draine (1993) for silicate and graphite dust, averaged over a Planck spectrum of $T = 12000\,{\rm K}$.[12] We also assume a specific gravity of $2.2\,{\rm g\,cm^{-3}}$ for graphite and $3.3\,{\rm g\,cm^{-3}}$ for silicates. These assumptions yield maximum values of $Q_{\rm pr}/a\rho \lesssim 19(4)$ for graphite (silicate) grains. For $T \approx 10000\,{\rm K}$ and $T \approx 8000\,{\rm K}$ these values are 16(3) and 13(2), respectively. These values determine the *maximum* radius to which grains could levitate; but grains of different sizes will levitate to different radii, owing to their range in $Q_{\rm pr}$.

For a general grain mass-size distribution in mass $dm(a)/da$ and absorption efficiency $Q_{\rm pr}(a)/a$, we can derive an approximate form of $W^{\rm grp}(r,h^{\rm dust})dr$ by assuming a flat galactic rotation curve, i.e. $M_{\rm tot}(r) \propto r$. Then the force balance equation (Eq. 9) gives $r = KQ_{\rm pr}(a)/a$ for some proportionality constant K, and we can take

$$W^{\rm grp}(r) = \int_{a_{\rm min}}^{a_{\rm max}} da \frac{dm(a)}{da} \delta(r - KQ_{\rm pr}(a)/a), \qquad (20)$$

that should accurately capture the mass distribution of levitating grains with a given grain-size distribution. For the $Q_{\rm pr}$ values of Laor & Draine with $T = 12000\,{\rm K}$, and the 'PED' grain size distribution of Kim, Martin & Hendry (1994; see § 2.5), the derived $W(r,h)$ can be reasonably fit by a second-degree polynomial, which is used in the actual algorithm.

The default value of C_f will be taken as the value necessary to give $F_{\rm IR}/F_{\rm opt} \simeq 1$ in the background radiation, and the default IMF is Scalo (1986), from $0.1\,M_\odot$ to $125\,M_\odot$.

The fiducial parameter values just described are summarized in Table 2 and are used in the fiducial models listed in Tables 5, 6, and 8.

[12] We do not account for the effect of extinction on the effective temperature of the escaping radiation.

TABLE 2
PARAMETERS FOR DUST EJECTION

Parameter	Description	Default value	Range
$Y_{\rm ej}$	fraction of metals distributed non-locally	0.5	0.0-1.0
$f^{\rm ej}_{\rm dust}$	portion of ejected metals in dust	1.0	0.0-1.0
$Q_{\rm pr}/a\rho$	absorption efficiency for dust	$19(G), 4(S)$	-
C_f	free constant in dust correction	fixed by $L_{\rm IR}/L_{\rm opt}$	-
correction	dust correction type	Z	$Z/L_{\rm bol}$/constant
IMF	IMF for L/M determination	Scalo	Scalo/Salpeter

2.4. *Other Parameters and Considerations*

A few more general considerations (and their associated parameters) are common to two or more of our prescriptions and we discuss them here. The total normalization of the metal mass in our calculations is given by the 'effective yield' y_*, defined as the ratio of metal mass returned to the ISM to the stellar mass formed, in solar units. We take y_*=1 (i.e. solar yield) for all runs both because this is conventional and because all results can be simply scaled to a different effective yield.[13] As discussed later, a higher overall effective yield may in fact be called for by the observations (see also Renzini 1997; Pagel 1999; Aguirre 1999).

The yield y_* is split into gaseous metals and metals locked in dust. For metals distributed in the local gas, we take the ratio $f_{\rm dust} \equiv$(dust mass)/(total metal mass)$= 0.5$, as in local galaxies, and as suggested by observations of damped Ly-α absorbers (Pei, Fall & Hauser 1999; but see Pettini et al. 1997 for a lower estimate). For ejected metals, we allow a different ratio $f^{\rm ej}_{\rm dust}$. For wind ejection, we should have $f^{\rm ej}_{\rm dust} \lesssim f_{\rm dust}$, which is sensible if most of the ejected metal mass is in the ISM of the galaxy that has been entrained by the wind (it is an upper limit because some dust would be destroyed during ejection). The value may be somewhat different – in a quite unknown way – if most metals are contained in the hot wind itself. For radiation pressure ejection, $f^{\rm ej}_{\rm dust} \lesssim 1$ applies; the fraction then represents the survival fraction of dust as it traverses the halo during its ejection.

The fraction $Y_{\rm ej}$ of metals that are ejected (versus locally distributed) could vary anywhere from near zero, for radiation pressure ejection where gas drag or magnetic confinement is very strong, to near one or more for galactic-scale winds where the metal-rich supernova ejecta escapes along with some entrained gas. We use a fiducial value of $Y_{\rm ej} = 1$ for 'superwinds', and $Y_{\rm ej} = 0.5$ for quiescent winds. For dust, $Y_{\rm ej} > 0.5$ could not be maintained for much of a galaxy's lifetime since only $\sim 1/2$ of a typical galaxy's metals are in dust at any given time, and even values of $Y_{\rm ej} \sim 0.5$ would severely change the abundance ratios of refractory vs. non-refractory elements in the galaxies. Hence, this is probably an upper limit.

A final parameter ϵ_* is introduced in an effort to correct for a possible disparity between the simulations and reality: whereas the simulations tend to find $\Omega^{\rm sim}_*(z = 0) \gtrsim 0.011$, values of $0.002 \lesssim \Omega^{\rm obs}_*(z = 0) \lesssim 0.006$ are estimated from observations (e.g., Fukugita, Hogan & Peebles 1998). Three possible reasons for this disparity (discussed in §4) are: 1) The simulation Ω_* is correct but most of the 'stellar' mass is unobservable, e.g., brown dwarfs, 2) the simulations over-estimate the efficiency of star formation, or 3) the observations underestimate Ω_*. In cases 1) and 2), the simplest reasonable correction to make is to multiply the SFR and the luminosity of the simulation galaxies by $\epsilon_* = \Omega^{\rm obs}_*(z = 0)/\Omega^{\rm sim}_*(z = 0) \gtrsim 0.011 \approx 0.36$ wherever they are used. The stellar yield y_* should also be multiplied by ϵ_*, although if case 2) holds the resulting stellar metallicities will be too low.

2.5. *Treatment of Dust and Dust Destruction*

Our method incorporates a fairly detailed treatment of IG dust. We track both the dust mass and grain-size distribution for each gas particle, and treat the conversion of dust to gaseous metals by thermal sputtering. Dust is added to pristine gas with a set grain-size distribution, but when adding dust to a gas particle that has dust, we average the grain size distributions.

The extinction properties of dust in galaxies appear to be well fit by models employing spherical grains with a power-law grain-size distribution. The grain sizes necessary to account for the extinction data range from $a_{\rm min} \sim 0.001\,\mu$m up to some cutoff (generally either sharp or exponential) above $\sim 0.2\,\mu$m. We represent the grain-size distribution by a set of power laws, i.e.

$$\frac{dN(a)}{da} \propto a^{\alpha_k - 3} \quad \text{for } a_k \le a < a_{k+1},\ k = 1..N, \qquad (21)$$

for some set of α_k, with $dN(a)/da$ a continuous function. We implement this by tracking the dust mass $d_k(i) \equiv dm^{\rm dust}_i(a_k)/da$, where i is the particle number. The differential dust mass values at the selected set of a_k then determine the shape of the grain size distribution; clearly for $N \to \infty$ this allows for an arbitrary grain-size distribution; but in practice the method is 'efficient' enough that a small number ($N \sim 9$) provides good accuracy (see the upper panel of Figure 1 for a demonstration).

The total dust mass in a particle is determined by a

[13] The metallicity-dependent dust correction in the radiation-pressure prescription does depend on y_*, but the effect is largely counteracted by changing C_f to ensure the proper $F_{\rm FIR}/F_{\rm opt}$ in the derived optical and FIR backgrounds.

TABLE 3
GENERAL PARAMETERS

Parameter	Description	Default value	Range
y_*	mean stellar yield (solar units)	1	-
$\epsilon_\star$	factor multiplying SFR, $\dot{m}_{\rm out}$, $L_{\rm bol}$	1.0	0.355-1
$f_{\rm dust}$	portion of locally-distributed metals in dust	0.5	-

piecewise power-law integration over d_k, i.e.

$$m_i^{\rm dust} = \sum_{k=1}^{N-1} \frac{d_k(i)}{\alpha_k + 1} \left[\left(\frac{a_{k+1}}{a_k} \right)^{\alpha_k} a_{k+1} - a_k \right] \qquad (22)$$

where $\alpha_k = \log(d_{k+1}/d_k)/\log(a_{k+1}/a_k)$. For $\alpha_k - 1 < \epsilon \approx 10^{-4}$ a term in the sum is replaced by $d_k(i) a_k \log(a_{k+1}/a_k)$, which is good to $O(\epsilon^2)$.

To add dust to a particle, we simply add to the $d_k(i)$ values of the assumed grain size distribution at a_i, such that the total mass corresponding to the added distribution is equal to the desired additional dust mass. This in general will *not* give a set of d_k that yield the correct total mass (though it will be close), so we 'renormalize' the entire distribution, since the total mass scales with a constant multiplying all the $d_k(i)$. This effectively yields a 'best fit' of the two summed piece-wise power-law distributions using a third with the same mass. A sample addition is shown in Fig 1 (lower panel).

For dust destruction, we find the sputtered radius a_s using the gas temperature and density from the simulation, the time interval since the last simulation output, and the thermal sputtering yields of Jones et al. (1994). The grain distribution is then transformed by $dN(a)/da \rightarrow dN(a+a_s)/da$, or in practice $d_k \rightarrow d'_k$, where the latter is given by a power-law interpolation:

$$d'_k = d_j \left(\frac{a_k + a_s}{a_j} \right)^{\alpha_j} \left(\frac{a_k}{a_k + a_s} \right)^3 ,$$

where j is selected so that $a_j \leq a_k + a_s < a_{j+1}$. For $j \geq N$ we use $j = N - 1$, i.e. extrapolation. The fraction of dust destroyed could then be calculated by integrating this new set of d'_k and comparing to the old. This gives a good approximation to the effect of thermal sputtering on the dust mass and grain-size distribution. We have not calculated non-thermal sputtering of the grains (because it requires grain velocities), but it could be important: the grain velocity $v_{\rm dust}$ would, in the grain's rest frame, correspond roughly to a temperature of $6 \times 10^5 (v_{\rm dust}/100\,{\rm km\,s^{-1}})^2\,K$.

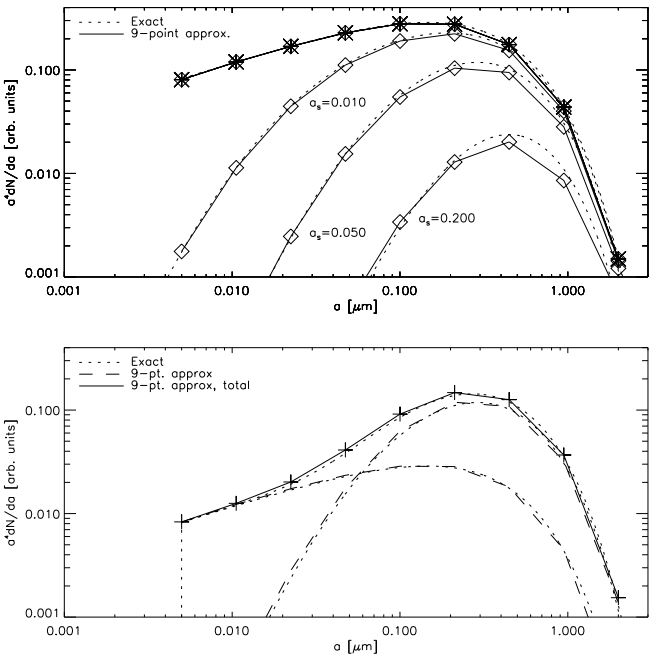

FIG. 1.— Demonstration of the dust treatment. **Top:** Unsputtered (stars) and sputtered (diamonds) grain-size distributions, for several values of the sputtered radius, a_s, for graphite grains. Dotted lines show the exact distribution; solid lines show the simulations representation using 9 points. **Bottom:** sputtered distribution with $a_s = 0.05\,\mu$m added to an unsputtered distribution with half the mass, yielding a new grain-size distribution (solid). Exact solutions are dotted, 9-point approximations are dashed and solid.

In this study, for the grain-size distribution we use the 'power-law exponential decay' (PED) fits of Kim, Martin & Hendry (1994) of $N(a) \propto a^\alpha \exp(-a/a_c)$. They give $\alpha = -3.48, a_c = 0.28\,\mu$m for graphite, and $\alpha = -3.06, a_c = 0.14\,\mu$m for silicates.

While the dust treatment employed here is fairly accurate, it currently has a few limitations:

1. The dust destruction is underestimated in the simulations because we have neglected non-thermal sputtering, and dust destruction during ejection. Therefore, we only compute dust destruction correctly *after* the grains have come to rest in the IGM.

2. Dust destruction may also be underestimated if dust encounters very dense, hot regions for shorter time intervals than the interval between the simulation outputs. for example, this could happen for dust cycling through cluster cores.

3. We currently only treat one grain species at a time,

TABLE 4
PARAMETERS FOR DUST TREATMENT

Parameter	Description	Default value	Range
$a_{\rm min}$	minimal grain size	$0.005\,\mu$m	-
$a_{\rm max}$	maximal grain size	$2.0\,\mu$m	-
dust type	dust chemical composition	graphite	graphite/silicate
GSD	grain-size distribution	PED	-

and add dust to gas with a fixed grain-size distribution, even though in a realistic ejection scenario dust should be somewhat segregated by size due to differences in grain absorption efficiencies and gas drag.

3. OBSERVATIONS CONCERNING COSMIC METALS

Sections 23-7 will discuss the models we have run, and the results obtained. First, however, it will be useful to briefly review the existing observations concerning cosmic metallicity.

3.1. *Cluster and Group Metallicity*

Measurements of elemental abundances using X-ray line emission have revealed that the intracluster medium of rich galaxy clusters is highly enriched, to between 1/3 and 1/2 solar metallicity (e.g., Mushotzky et al. 1996). Because the intracluster gas mass in a typical rich cluster exceeds the stellar mass in cluster galaxies by a factor of $\sim 5-10$ (e.g., Renzini 1997), this implies that cluster galaxies have probably ejected a large fraction (possibly up to three quarters) of their metals.[14] It also seems that a super-solar yield is necessary to account for all of the metals, since dividing the total cluster metal mass by the total stellar mass in the cluster gives a yield of $y_* \sim 2-4$ (Renzini 1997; see also Aguirre 1999). It should be noted that measured cluster metallicities are emission-weighted and favor the cluster cores; strong radial metallicity gradients would imply a different mean metallicity for the cluster. Cluster abundance gradients are currently somewhat inconclusive (see Renzini 2000), but seem to be weak except in clusters with strong cooling flows (White 2000; Finoguenov, David & Ponman 1999).

While there is general agreement that in the cores of clusters at $z \lesssim 0.3$ the gas typically has roughly constant $Z/Z_\odot \approx 0.3-0.5$ for cluster temperatures down to $\sim 3.0\,$KeV (e.g., Renzini 1999), the observed enrichment of cooler clusters and groups is less secure. Davis, Mulchaey & Mushotzky (1999) find that $Z/Z \sim 0.3$ for intra-group gas persists down to temperatures $T \sim 1.5\,$KeV, but for cooler groups the metallicity – and perhaps also the baryon fraction – declines, perhaps implying that winds can remove metals even from groups. Buote (2000), however, finds that two temperature models fit the X-ray data better than the one-temperature models used by Davis et al. and others—these fits yield significantly higher abundances in groups ($Z/Z_\odot \sim 0.5-1$). Well-resolved observations using *Chandra* should provide much firmer data on the enrichment properties of groups.

3.2. *Metals in Ly-α Absorbers*

A very useful window into the chemical enrichment of the IGM is provided by studies of quasar absorption lines. It is now widely accepted that the 'forest' of Lyα lines found in the spectra of $z \gtrsim 2$ quasars is due to absorption by a smoothly fluctuating neutral hydrogen component of the IGM (e.g. Cen et al. 1994; Zhang, Anninos & Norman 1995; Hernquist et al. 1996). Although these absorbers were initially expected to be pristine, high resolution spectroscopy has unambiguously identified metal lines (chiefly CIV and SiIV) associated with $N(H\,I) \gtrsim 10^{14.5}\,{\rm cm}^{-2}$ absorbers (e.g., Cowie et al. 1995; Songaila & Cowie 1996; Cowie & Songaila 1998; Ellison et al. 2000). Applying an ionization correction to the abundances derived from the line column densities (relative to the absorbers' H I column densities), and using a correlation between the Lyα column density and gas overdensity from numerical simulations, these lines can give useful information about the metallicity of the low-density component of the IGM. All of the absorption line studies essentially agree on an inferred metallicity of $Z/Z_\odot \sim 10^{-2.5}$ for $2.5 \lesssim z \lesssim 3.5$ absorbers with $N(H\,I) \gtrsim 10^{14.5}\,{\rm cm}^{-2}$, with about an order of magnitude scatter in the metallicity for different absorbers (e.g., Songaila & Cowie 1996; Rauch, Haehnelt & Steinmetz 1997; Songaila 1997; Hellsten et al. 1997; Davé et al. 1998). However, the metallicity of lower column density regions, corresponding to physical overdensities $\rho/\bar{\rho} \sim 1$, which would represent the bulk of baryonic matter at $z \sim 3$, is more uncertain. The metal lines corresponding to the low-column density Ly-α absorbers are generally too weak to detect directly and their presence can only be derived in a statistical sense, e.g., by analyzing the median absorption per pixel (Cowie & Songaila 1998). Recently, Ellison et al. (2000) used a very high quality quasar spectrum to show that the CIV enrichment must extend to column densities significantly lower than $N(H\,I) = 10^{14.5}\,{\rm cm}^{-2}$. Schaye et al. (2000) demonstrated that OVI is a more sensitive probe of the metallicity in low-density gas than CIV. Using a pixel analysis, they detected OVI in gas with $\tau(HI) < 1$, which corresponds to gas densities around the cosmic mean. (See, also, Hellsten et al. 1998; Davé et al. 1998.)

In summary, the typical metallicity of the high column density IGM is 10^{-3} – 10^{-2} solar. Very little is known about the variation and the scatter of the metallicity as a function of density. Although the presence of metals in the low-density IGM has been established using statistical

[14] If a significant fraction of cluster stars are intergalactic, the factor might be reduced, but galaxies must still lose $\sim 1/2$ of their metals.

techniques, both the overall mean metallicity of the IGM and the fraction of the IGM that is enriched have yet to be determined.

3.3. *Metals in Galaxies*

To develop a consistent theory of cosmic metallicity, one must take into account not only metals in the IGM, but also metals distributed in and near the metal-forming galaxies. The chemical properties of galaxies constitutes a vast subject (see, e.g., Pagel 1997), and here we will only summarize some observations that will be of use in evaluating the results of our simulations.

The abundances of heavy elements in galactic gas and stars are known to vary with galaxy mass or luminosity and galactic radius, and perhaps galaxy type. All three effects are evidenced in the very useful compilation by Zaritsky, Kennicutt & Huchra (1994). They note that nearly all observed galaxies demonstrate radial abundance gradients, making it difficult to assign a particular metallicity to a galaxy. However, by choosing a 'characteristic' radius (either an isophotal radius or the disk exponential scale length), they can compare abundance properties of various galaxies at that radius. This reveals a strong metallicity-luminosity relation (see Eq. 15 above and Zaritsky et al., Figure 13) for $[O/H]$ in spiral H II regions. A similar but shallower M-Z relation exists in $[Fe/H]$ in stars in ellipticals (Zaritsky et al. 1994; Kobayashi & Arimoto 1999). In both cases the characteristic metallicity can range from $\ll 1/10\,Z_\odot$ in the smallest galaxies to several times solar in the largest. These relations can be meaningfully compared to the gaseous and stellar metallicities in the simulation galaxies at $z = 0$, although we do not have information on the Hubble type of the simulation galaxies.

At high redshifts, data concerning the chemical properties of galaxies can be gleaned from observations of Lyman-break galaxies or from studies of damped Lyα absorbers. Unfortunately, metallicity information about Lyman-break galaxies is extremely limited (Pettini et al. 2000) and we cannot make a meaningful comparison with our simulation metallicities at $z = 3$. The damped Lyα absorbers constitute the highest column density ($N(HI) \gtrsim 10^{20}\,\mathrm{cm}^{-2}$) features of QSO absorption spectra. Abundances have been measured for many of these systems, giving metallicities of $\sim 1/30 - 1/10$ solar (e.g., Pettini et al. 1999; Prochaska & Wolfe 2000). It is unclear, however, exactly what sort of systems the damped Lyman absorbers represent; they may arise from a diverse population of objects (e.g., dwarf galaxies, outer disks of spirals, etc.; see Pettini et al. 1999 and references therein). Since we cannot draw a one-to-one relation between these objects and an overdensity or average density of a galaxy, we will not compare our simulations to these observations in the present study.

4. GALAXY MASSES AND STAR FORMATION RATES IN THE SIMULATIONS

In this study we apply the method described in § 2 to three SPH simulations, performed using the method described by Katz, Weinberg & Hernquist (1996). The simulations themselves are described more specifically in Murali et al. (2001). Briefly, all three use parameters $\Omega_m = 0.4 = 1 - \Omega_\Lambda$, $\Omega_b = 0.02h^{-2}$, $\sigma_8 = 0.8$ and $h = 0.65$. The first simulation has 144^3 gas and 144^3 dark particles in a $(50\,h^{-1}\,\mathrm{Mpc})^3$ box, giving a dark particle mass of $6.3 \times 10^9\,\mathrm{M}_\odot$ and a gas particle mass of $8.5 \times 10^8\,\mathrm{M}_\odot$. The other simulations are both $(11\,h^{-1}\,\mathrm{Mpc})^3$ in volume, and use 2×128^3 and 2×64^3 particles, respectively. The 128^3 simulation has dark and gas particle masses of $9.8 \times 10^7\,\mathrm{M}_\odot$ and $1.3 \times 10^7\,\mathrm{M}_\odot$, respectively. The smaller simulation boxes stop at $z = 3$, and most conclusions regarding the universe at $z = 3$ will be drawn from these. The 144^3 simulation runs down to $z = 0$. The 128^3 and 64 simulations include an ionizing background of from Haardt & Madau (1996) (attenuated by a factor of two to adjust for our assumed Ω_b; see Weinberg, Hernquist & Katz 2000), whereas the 144^3 simulation does not.

For our method to yield useful results, it must be applied to simulations that can reasonably reproduce the mass, luminosity, and SFR distributions of observed galaxies. Here we briefly discuss the comparison of the simulation mass function and SFR to observations and their role in our predictions (for more details see Weinberg et al. 1999, 2000; Murali et al. 2001; Katz et al., in preparation, Bullock et al., in preparation). The luminosity function, which is generated in our calculations of radiation-pressure ejection, is discussed in § 7.

The simulations yield a mass function of galaxies directly. An 'observational' mass function can be constructed using an observed luminosity function and a prescription for converting light to mass. Using either a constant $M/L_B = 7.5$ (in solar units) or a M/L_B function derived by Salucci & Persic (1999; Persic & Salucci 1997), the mass function from the 2dF survey (Folkes et al. 1999)[15] survey shows quite good agreement – in both shape and normalization – with the 144^3 simulation for galaxy (gas+star) masses between $10^{10.5}\,M_\odot$ and $10^{11.75}\,M_\odot$ (Katz et al., in preparation). At lower masses, galaxies are unresolved by this simulation: as shown by Weinberg et al. (1999), only galaxies with $\gtrsim 60$ SPH particles are well resolved; this corresponds to baryonic masses of $5.1 \times 10^{10}\,\mathrm{M}_\odot$ in the 144^3 simulations and $7.9 \times 10^8\,\mathrm{M}_\odot$ in the 128^3 runs. At higher masses the simulation exhibits a significant excess of galaxies. This may result from inaccuracies in the mass-to-light conversion for very massive galaxies, or from incompleteness of the surveys (e.g., due to surface brightness effects; see Impey & Bothun 1997), or due to differences in the way masses of real and simulated galaxies are estimated, or due to overproduction of massive galaxies in the simulations. The last two uncertainties are exacerbated by the special environments of the largest galaxies, most of which are found in cluster cores.

When integrated, the simulation mass function for the 144^3 runs yields a cosmic density in stars of $\Omega_*(z = 0) = 0.011$. This is somewhat higher than the value of $\Omega_* = 0.004 \pm 0.002$ derived by Fukugita et al. (1998) from observed luminosity functions, or from the integrated SFR of Steidel et al. (1999), which yields $\Omega_* \approx 0.006$. Likewise, the simulation SFRs both at low and high redshift tend to exceed the observed values (see Weinberg et al. 1999). A similar discrepancy was noted based on earlier simulations by Katz et al. (1996) and by Pearce et al. (1999). These discrepancies may be caused by an observational underes-

[15] The ESO slice project results of Zucca et al. (1997) are very similar.

timate of $\Omega_*(z=0)$ and of the SFR (due, for example, to surface brightness effects or high production of low-mass, dim stars), and/or by simulation galaxies being too massive by some roughly constant factor, and/or by the overproduction of certain galaxies in the simulations.[16]

In summary, all of the simulations fail to resolve the fraction of the mass function below the simulation resolution limit. At the same time, the simulations may nevertheless *over*predict the number and/or mass of galaxies that are resolved. We will address these issues in detail in future papers (Katz et al., in preparation; Bullock et al., in preparation; see Weinberg et al. 1999 for preliminary discussion), but note for the present that the large SFR and possible overabundance of galaxies we find could result from the single-phase description of the gas in the simulations, or from the lack the of strong feedback. Feedback could suppress star formation both in the wind-driving galaxy and in nearby galaxies (see Scannepieco & Broadhurst 2000 for some discussion of the latter effect), but there is no good way to model such feedback using our current methodology. If enrichment were caused mainly by dust ejection, dynamics or metal-rich, quiescent winds, our neglect of the winds' effect on the galaxies would be more self-consistent, though effects other than strong feedback would then be required to suppress any excess of small galaxies.

Any real disagreements between the simulations and reality will clearly affect the accuracy of the IGM enrichment calculations of this study. We test a possible way of compensating for such disagreements by including a parameter ϵ_* that can multiply the SFR (which effectively sets the supernova rate in our method), the yield y_*, and the luminosity of the groups. With $\epsilon_* = \Omega_*^{\rm obs}/\Omega_*^{\rm sim}$, this would be an accurate adjustment if the discrepancy were due to hidden low mass stars, since most of the radiation, metal and energy comes from the most massive stars. If simulation galaxies are simply more massive by a constant factor $\Omega_*^{\rm sim}/\Omega_*^{\rm obs}$, the same adjustment would properly account for the different galaxy luminosities, galaxy SFRs, and overall enrichment of the universe. However, since the galaxies would still have their original unadjusted masses, we would effectively *over*estimate the effect of gravitation as well as underestimate the SFR per unit mass in the galaxies. Finally, if the 'observed' values are underestimated (and the simulations correct), no adjustment is necessary; the galaxies *that the simulations resolve* would be like their counterparts in reality. However, as noted above it seems likely that the low-mass galaxies (at least) are significantly overproduced in the high resolution simulations at $z \geq 3$.

5. RESULTS FOR DYNAMICAL REMOVAL

The removal of metal-enriched gas from galaxies by dynamical processes has been studied in the context of clusters (e.g., Fukumoto & Ikeuchi 1996; Abadi, Moore & Bower 1999; Quilis, Moore & Bower 2000), and in the cosmological context (Gnedin & Ostriker 1997; Gnedin 1998; Cen & Ostriker 1999). Gas may be removed during a close interaction between two or more galaxies in which a fraction of the gas attains escape velocity (see, e.g., Barnes & Hernquist 1992). Alternatively, loosely bound gas may be stripped from a galaxy by the ram pressure of the IGM through which the galaxy is moving. Removal of metals via mergers or tidal disruption may occur in clusters or in the general IGM, whereas ram-pressure stripping is probably only important in massive clusters.

We have applied the method of § 2.1 to our simulations to examine the dynamical removal of metals. Metals are deposited only in bound groups, thus by calculating the IGM enrichment at later times we can directly assess the amount of metals that can be removed by dynamics alone. The results of these trials are shown in Table 5 and Figs. 2 and 3. The table gives the overall fraction of metals that are outside of bound groups, the metallicity of the IGM at its mean density and at an overdensity $\delta \equiv \rho_{\rm gas}/\langle\rho_{\rm gas}\rangle = 100$, and the mean stellar metallicity in galaxies. Unless otherwise noted, we include both gaseous metals and dust in computing the metallicities (for dynamical and wind enrichment, this is at very worst a factor of two larger than if dust is not included; for dust ejection we show dust and gaseous metal fractions independently).

Figure 2 shows the mean metallicity $\langle Z_\delta\rangle$ of the IGM as a function of δ, and the mean metallicity of hot ($> 5\times10^6\,{\rm K}$) bound cluster/group gas as a function of gas temperature. Since the clusters tend to have radially declining temperature gradients, the plotted cluster temperatures are lower than the core temperatures; we have also plotted the mean temperature of the ICM within 100 kpc for the hottest five clusters. Note also that the cluster gas metallicity is slightly overestimated because some hot gas associated with galaxies is included, but an examination of radial metallicity profiles indicates that the effect is small.

The mean metallicity vs. overdensity should be interpreted with care; for a highly inhomogeneous metal distribution, the mean can be dominated by a few highly enriched particles and should not necessarily be compared to the 'typical' metallicity found in Lyα absorbers. The median particle metallicity gives a better estimate of typical *particle* metallicities, but since each observed line would correspond to gas represented by a number of particles, the median metallicity of absorption systems should probably be higher than the median for particles (for a highly inhomogeneous distribution). Thus we expect that the mean and median particle metallicities should lie above and below the metallicity that should be compared to 'typical' observed metallicities at a given column density (see Aguirre et al. 2001b for more discussion). In this paper we display mainly mean metallicities, which should be considered upper limits.

The results show that dynamical removal is rather inefficient, removing only a few percent of a typical galaxy's metals over its lifetime. The enrichment, as clearly shown in Fig 2 (dot-dashed line), is insufficient to account for the metallicity of Ly-α absorbers at $z\sim3$, which have $Z \approx 10^{-2.5}\,Z_\odot$ down to at least $N(HI) \approx 10^{14.5}\,{\rm cm}^{-2}$.

These results are in substantial agreement with simulations of individual galaxy interactions, which tend to show that only a few percent of an interacting galaxy's mass can attain escape energy during an encounter (Barnes 1988; Barnes & Hernquist 1992; Hernquist 1992, 1993). Our

[16] The high-resolution runs seem to over-produce small galaxies at $z=3$ as compared to the luminosity function computed by Steidel et al. (1999).

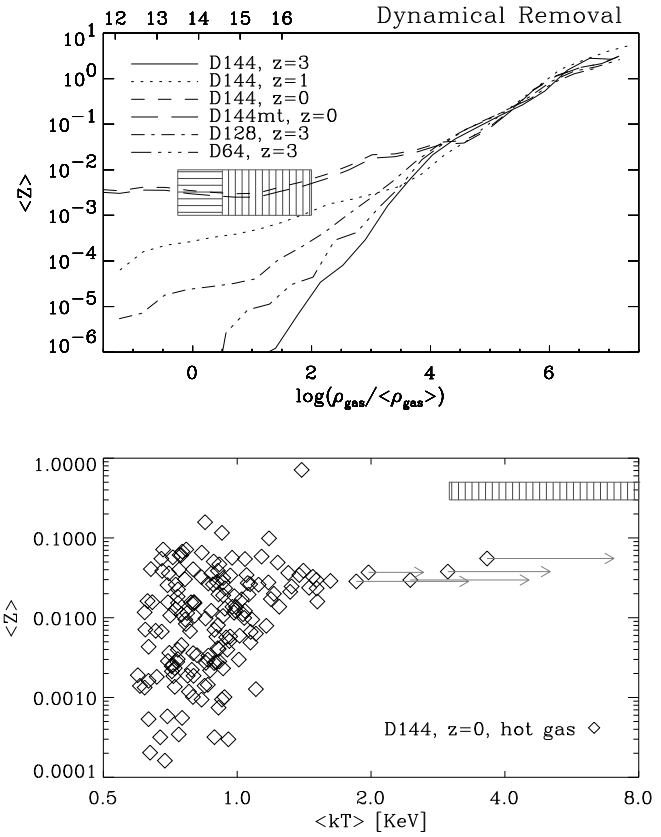

FIG. 2.— Enrichment of the IGM for dynamical removal of metals. **Top:** Mean metallicity $\langle Z \rangle$ vs. overdensity for the three simulations at $z = 3$, and for the 144^3 simulation at $z = 0$. Also plotted is the $z = 0$ 'D144mt' model as a time-resolution test. The top axis is $\log N(H\,I)$ (cm^{-2}) of an absorber corresponding to the bottom-axis overdensity *at* $z = 3$, using the Davé et al. (1999a) relation. The vertically striped box outlines the approximate current constraints from the Lyα forest at $z \approx 3$ while the horizontally striped box shows an extension of these constraints to lower densities (see discussion in § 4). **Bottom:** Group/cluster mean metallicity (in hot gas) vs. mean temperature of hot bound gas at $z = 0$. Arrows show the mean temperature of hot gas in the central 100 kpc for the hottest clusters. The vertically striped box outlines the approximate constraints from cluster X-ray studies.

results are somewhat in disagreement with those of Gnedin (1998), who found – using high resolution SLH-P^{3}M simulations at $z \gtrsim 4$ – that dynamical enrichment was more effective than supernova-driven ejection, and also sufficient to enrich the low-density IGM. While our results support the general idea that *some* metals escape into the $z = 3, \delta < 100$ IGM through dynamics alone, we find that the amount is negligible compared to the other mechanisms we consider. We cannot rule out the possibility that small (unresolved by our simulations), quickly merging galaxies at $z \gg 5$ could enrich the IGM more than our calculations suggest; this would, however, require more *efficient* ejection (or a very super-solar yield at high z), since if only a few percent of metals are ejected and mixed thoroughly, at least 10% of gas must form stars with solar yield to give a uniform enrichment of $\sim 10^{-2.5}\,Z_\odot$.

The metallicity of the gas in rich clusters in the 144^3 run is an order of magnitude below the observed value of $\approx 0.3 - 0.5\,Z_\odot$ (see § 3), from which we can conclude that dynamical removal of metals from massive galaxies ($\gtrsim 10^{10.5}\,M_\odot$) cannot account for the metallicity observed in cluster gas. Since ram-pressure stripping should be most efficient in small galaxies, it is important to note that we cannot directly address the importance of pressure-stripping of dwarf galaxies in ICM enrichment. However, if this process is to account for the observed ICM enrichment, it must happen at rather high redshift, since the mass contribution of $M \lesssim 10^{10.5}$ M$_\odot$ galaxies at present is quite small, i.e. the enrichment would have to happen at a high enough redshift that the galaxy mass function had a significant fraction of mass in the small galaxies. Note also that we have neglected enrichment from Type Ia supernovae in intergalactic cluster stars. We do not expect this to be significant in the field because only a few percent of the simulation stars are intergalactic (having been moved into the IGM dynamically), but it may be more important in clusters, which may have more IG stars. This effect would be best treated by introducing 'delayed enrichment' into our simulations. Although inefficient (for the galaxies resolved), dynamical removal is more effective in clusters than in the field. Assuming that the ratio of cluster stars to cluster gas is comparable to the field value of $\Omega_*/\Omega_b \simeq 0.23$, the ejection fraction $f_{\rm ej,cl}$ in rich clusters is

$$f_{\rm ej,cl} \simeq \frac{\langle Z_{\rm cl} \rangle}{(\Omega_*/\Omega_b) y_*} \simeq 0.16 \qquad (23)$$

in the 'D144' model, as compared to 0.04 for all galaxies. (Though if stars form more efficiently in clusters, this fraction would be smaller.)

Panels 1 and 4 of Figure 3 give the average metallicity of stars and gas, respectively, as a function of galaxy mass. Interestingly, stellar and gaseous M-Z relations exist even though galaxies retain nearly all of their metals. The relations occur both because the smallest galaxies have higher gas fractions, and because they tend to be younger. These can be compared to the plotted lines that are rough fits to the mass-metallicity relations found by Zaritsky et al. (1994) for ellipticals and spirals spanning $\sim$ 15 B magnitudes.[17] Unfortunately the simulations only have enough dynamic range to probe the brightest four magnitudes. One should also be cautious about the properties of the smallest galaxies, near the resolution limit (vertical line). Nevertheless, the 'D144' model does seem to exhibit an M-Z relation that is too weak in stars, and the stars have significantly higher metallicity than observations indicate. More effective feedback would prevent stars from forming in high-metallicity regions but cannot cure the problem, since the metals would then be present in the gas – but the gaseous M-Z relation is quite close to the observations. Thus it seems that the observed M-Z relation very likely indicates metal ejection beyond pure dynamics. We can also see from these figures that although all the results are shown for a solar yield, the results cannot be scaled by changing y_* by a significant amount without clearly violating the observed abundances. Thus while it might be argued that dynamical removal of metals could pollute the IGM more than we predict given a much higher yield (presumably due to an IMF biased toward massive stars), this argument would require the higher yield to apply only at

[17]Since our simulations do not provide types for the galaxies, we treat all galaxies as spirals when comparing to the gas metallicities, and all as ellipticals when comparing to the stellar metallicities.

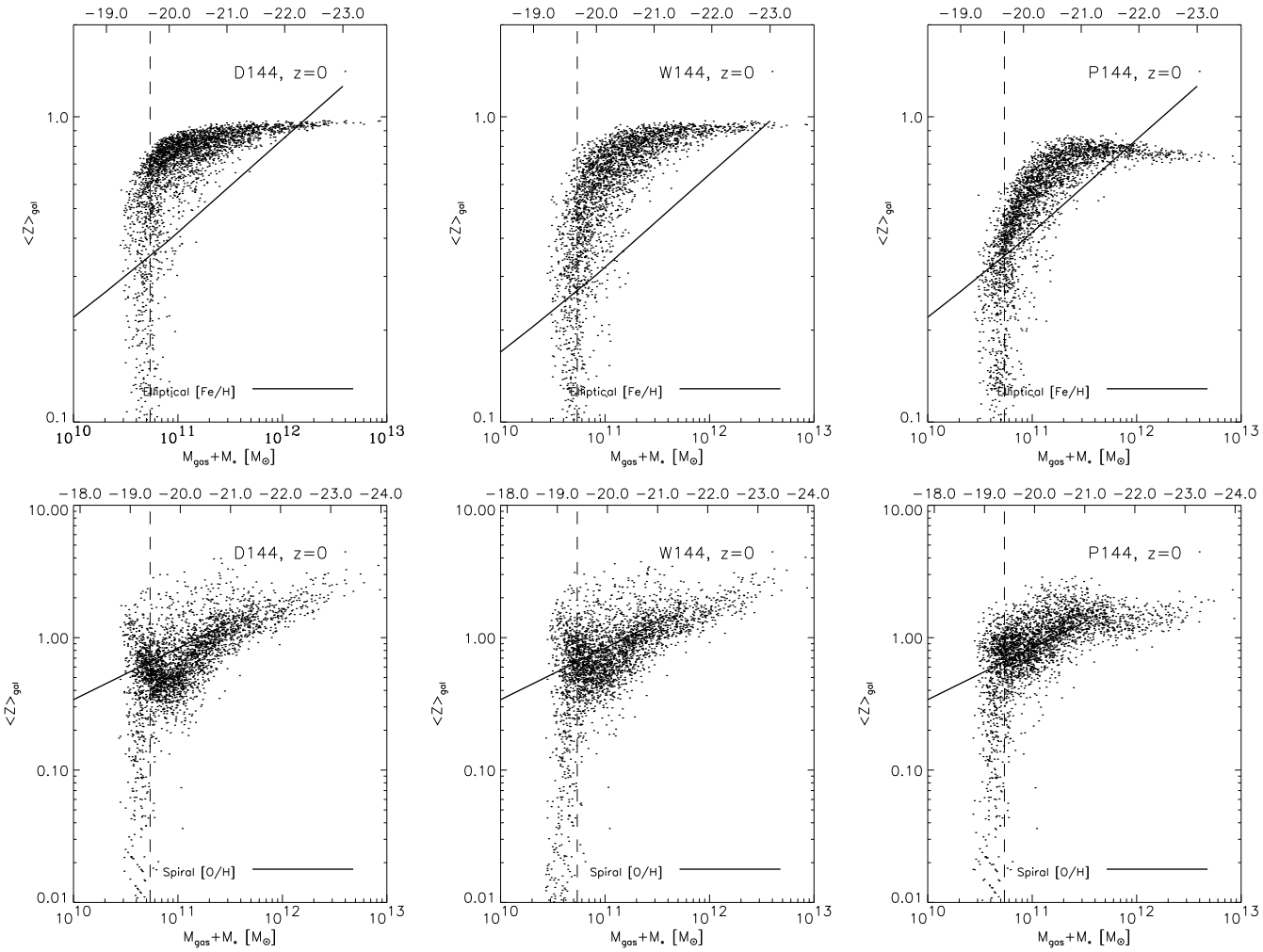

FIG. 3.— **Top three panels:** Mean stellar (top three panels) metallicity of galaxies in the fiducial dynamical, wind, and dust (resp. 'D144', 'W144' and 'P144') models at $z = 0$. Bottom axis shows stellar+gas mass, top axis shows B-band magnitude, converted from the mass using the elliptical galaxy relation from Persic & Salucci (1997). The solid line shows the elliptical [Fe/H] M-Z relation taken from Zaritsky et al. (1994). **Bottom three:** Average gas metallicity of galaxies at $z = 0$ for the same three runs. Bottom axis shows stellar+gas mass, top axis shows B-band magnitude, converted from the mass using the spiral galaxy relation from Salucci & Persic (1999); solid line is the spiral M-Z relation from Zaritsky et al. (1994). The mass of 64 gas particles is indicated by the vertical dashed line.

high-z, before the bulk of cosmic metals are formed.[18]

Our results concerning dynamical removal of metals are not weakened by the large uncertainties in the assumed parameters, since in this prescription only the yield y_* is important, and can be constrained within a factor of two. However, our predictions also are subject to some numerical uncertainties.

First, if the timescales for some dynamical processes that remove metals from galaxies were shorter than the time interval between the simulation outputs used, our prescription might not accurately treat their importance. We have checked this by repeating our calculation using 27 timesteps (model 'D144mt') rather than 19 (model 'D144'); the additional steps were chosen to roughly halve the interval between snapshots during the epoch when most star formation takes place ($1 \lesssim z \lesssim 3$). The differences between these two models are quite small (see Figure 2), indicating that even with 19 timesteps our calculations have numerically converged.

A numerical uncertainty that is harder to address is that caused by the limited resolution of the simulations themselves. An accurate assessment of the dynamical removal of metallic gas – whether during mergers, through tidal disruption, or via ram pressure stripping – depends on the ability of the simulations to accurately treat both the IGM and the structure of the galaxies. The mean physical interparticle spacing in our simulations is $133\delta^{-1/3}(1+z)^{-1}\,\mathrm{kpc}$ for the 128^3 runs and $534\delta^{-1/3}(1+z)^{-1}\,\mathrm{kpc}$ for the 144^3 runs (where δ is the gas overdensity), large compared to the scale of a typical galaxy. Moreover, the central 200 kpc of a cluster with $100 \lesssim \delta \lesssim 1000$ has only 200-2000 SPH particles; it is therefore doubtful that ram pressure effects on cluster galaxies are treated accurately (see Abadi, Moore & Bower 1999 for discussion). Unfortunately we cannot yet perform resolution tests as we have only one simulation complete to $z = 0$. Our simulations treat galaxy-galaxy interactions more accurately but still with limitations. Large, thick galaxies are probably represented well, whereas low mass galaxies and thin disks will not be captured. Therefore, while *in principle* our type of investigation can assess the efficiency of dynamical removal quite well, in practice we expect limitations due to limited resolution.

We have attempted to test this effect by comparing the efficiency of dynamical metal removal in the 64^3 and 128^3 runs with the restriction that metals are only added to gas particles in galaxies of a fixed mass range. For example, we may add metals only to galaxies with $60-120$ (gas+star) particles in the 64^3 run and only to galaxies with $480-960$ particles in the 128^3 run, to compare the relative efficiency of dynamical removal in galaxies with baryonic mass $6\times10^9 - 1.2\times10^{10}\,\mathrm{M}_\odot$ with different resolution. In this case, we find that $\approx 0.15\%$ of metals are lost by well-resolved galaxies in the 64^3 run by $z = 3$, whereas $\approx 1.7\%$ are lost in the 128^3 run. Curiously, we find that as we increase the mass cut for galaxies that receive metals, the ejection fraction *increases* in the 128^3 run, but *decreases* in the 64^3 run. The difference between the two runs can be accounted for either by a resolution effect (i.e. galaxies of the same mass lose different amounts of metals depending on the number of particles constituting them), or by the difference in the mass function of galaxies (i.e. the presence or absence of galaxies small compared to those with the metals). Were we to *assume* that in both runs most metals are lost from interactions between galaxies of comparable mass, then it would necessarily be a resolution effect. But if it were purely a resolution effect, it is very difficult to see why the ejection fraction would decrease with the number of particles in the 64^3 run while increasing in the 128^3 run. Thus we suspect that metal-loss from the massive galaxies is dominated by interactions with lower-mass galaxies in the 128^3 run, but dominated by interactions with other well-resolved galaxies in the 64^3 run (the small galaxies being absent). This dependence on the presence or absence of small galaxies makes our resolution test inconclusive.

6. MODELS AND RESULTS FOR WINDS

6.1. *Fiducial Wind Model*

As we discussed in § 2.2 there have been numerous investigations of galactic winds and their possible role in the enrichment of the IGM, and the chief empirical data concerning this process comes from observations of starburst-driven superwinds. Our fiducial wind model, labeled 'W' in Table 6 and in the figures, assumes an outflow velocity of $600 \pm 200\,\mathrm{km\,s^{-1}}$, with wind efficiency (defined by Eq. 4) $\chi = 1$, an entrainment fraction $\epsilon_{\rm ent} = 0.1$, and a critical SFR/(area) for driving a strong wind of $\mathrm{SFR}_{\rm crit} = 0.1\,\mathrm{M}_\odot\,\mathrm{yr}^{-1}\,\mathrm{kpc}^{-2}$. As described in § 2.2, these are chosen to match 'typical' values derived from the observations, where possible. Quantities that are not directly observable, such as $\epsilon_{\rm ent}$, the ejection fraction $Y_{\rm ej}$, and α (which controls the distribution that governs the placement of metals in the IGM) are given reasonable values that we vary in subsequent trials. The fiducial parameter values are listed in Table 1.

We show the results of our fiducial wind model in Tables 6 and 7, and in Figs. 3, 4, 5 and 7. We first focus on results at $z = 0$ from the 144^3 simulation. As listed in the first row of Table 6, the galaxies resolved by the 144^3 simulation lose about 6% of their metal mass to the IGM over their lifetimes. At $z = 0$, the mean metallicity of the IGM at its mean density, $\langle Z_{\delta=1}\rangle = 0.008\,Z_\odot$, $\langle Z_{\delta=100}\rangle = 0.02\,Z_\odot$, and the mean ICM metallicity for hot clusters is $0.04\,Z_\odot$. Figure 5 allows the most direct comparison to the principal results from the dynamical model, shown earlier in Figure 2, and reveals that winds can enrich the low-density IGM must more effectively than can the dynamical removal of metals.

Figure 4 shows some details as to how this enrichment occurs. The first panel plots the wind stalling radius $r_{\rm stall}$ as a function of galaxy mass, and shows that large galaxies with deep potential wells can retain their metals. Most galaxies resolved by the 144^3 simulation cannot drive winds past a few tens of kpc (smaller than the galaxies themselves), though a small fraction can drive metals hundreds or thousands of kpc into the IGM, where they eventually stall after flowing for up to a few Gyr (see panel 2). We have plotted all angles for each galaxy, so the vertical 'stripes' demonstrate the range of radii to which the shells propagate in different directions

[18] Note also that Pettini et al. (2000) find in their study of the $z = 2.73$ galaxy MS 1512-cB58 no evidence for a non-standard IMF.

TABLE 5
DYNAMICAL MODELS RUN

Model	Variation	$f_{\rm IGM}$	$\langle Z_{\delta=1}\rangle$	$\langle Z_{\delta=100}\rangle$	$\langle Z_{\rm cl}\rangle$	$\langle Z_{\rm gal}\rangle$
D144	-	0.038	0.0035	0.0064	0.036	0.87
D144mt	more outputs	0.037	0.0030	0.0051	0.032	0.87
D64	64^3	0.0025	$1.9 \times 10^{-7\dagger}$	4.6×10^{-5}	-	0.63
D64mt	64^3, more outputs	0.0023	$3.5 \times 10^{-9\dagger}$	4.3×10^{-5}	-	0.69
D128	128^3 run	0.017	2.4×10^{-5}	0.00035	-	0.75
D128lt	128^3, less outputs	0.017	2.5×10^{-5}	0.00040	-	0.61

Note: all results are given at $z = 0$ for the 144^3 run, and at $z = 3$ for the other two runs.
†In these runs average metallicities at $\delta \lesssim 10$ should not be trusted, since only a few particles have nonzero metallicity in this density range.

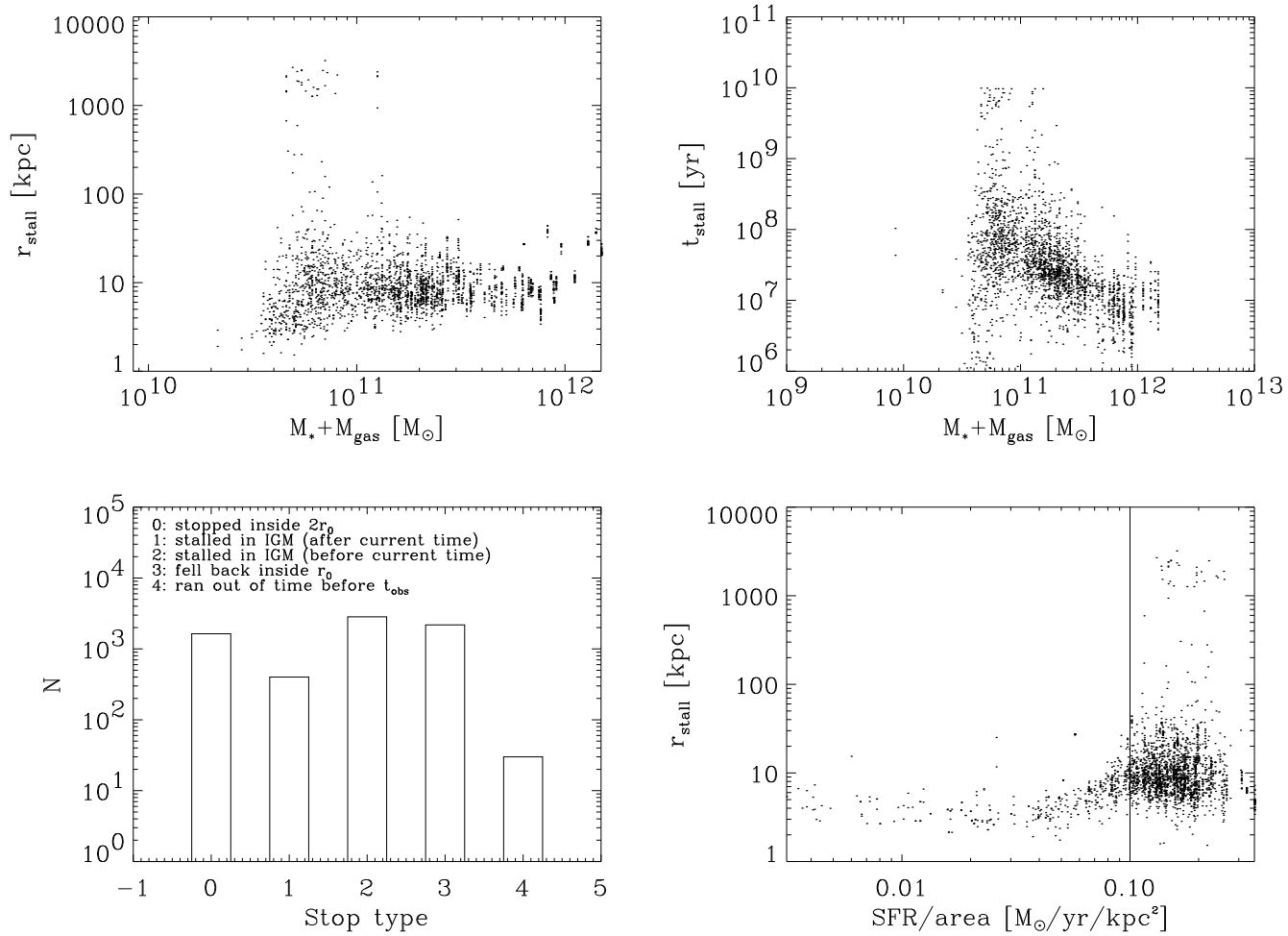

FIG. 4.— Quantities in wind ejection for fiducial 'W' model at $z = 1.5$. **Panel 1:** Physical shell stalling radius vs. galaxy mass. **Panel 2:** Time between the launching of a shell from r_0 and its stalling in the IGM. The cutoff at $\sim 10^{10}$ yr corresponds to $z = 0$. **Panel 3:** Histogram of the final fate of propagating shells. **Panel 4:** Shell radius vs. SFR/(area). The solid line indicates the critical SFR/(area).

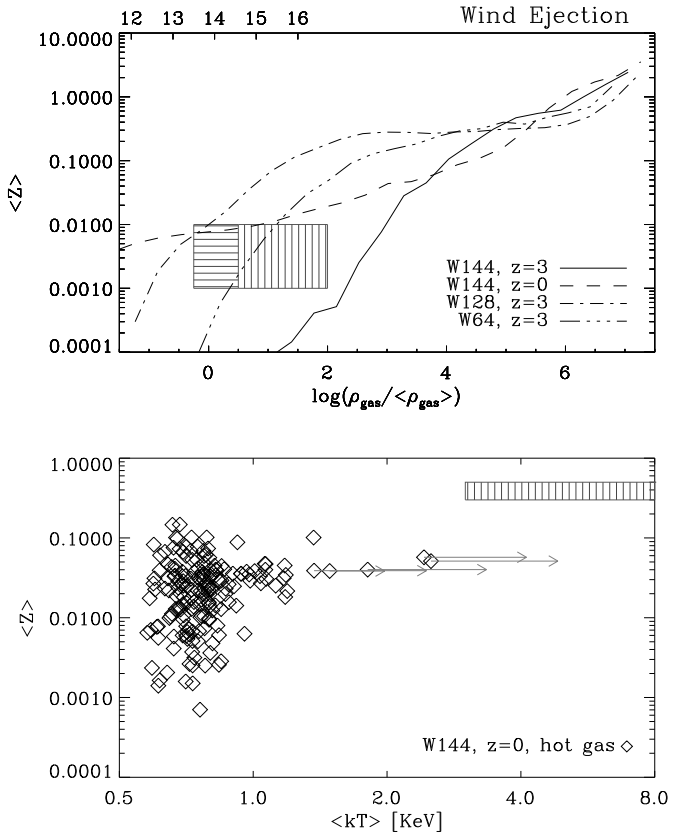

FIG. 5.— Enrichment of the IGM for the wind ejection of metals in the fiducial 'W' model (see Tables 1 & 6). Plotted quantities are as in Fig 2.

(typically 2-32 angles are used for each galaxy). Panel 3 histograms the final state of the shells ejected between $z = 1.75$ and $z = 1.5$. About 2/3 of the shells either stall within $2r_0$ or turn around and fall back to within r_0. Another third stall after $z = 1.5$, and a smaller fraction stall before $z = 1.5$ but after reaching $2r_0$. Finally, a small fraction are still propagating at $z = 0$. As shown in the last panel, most galaxies at $z = 1.5$ in the fiducial model are assumed to be driving winds (i.e. their SFR exceeds the assumed critical SFR), but even galaxies with very high areal SFRs may not drive an *effective* outflow, if they are very massive.

Figure 7 shows the details of the radial integration for one angle of one galaxy at $z = 1.5$. The first panel gives the shell, wind, infall and Hubble velocities and the IGM sound speed versus the shell radius. The shell, starting at $\sim 800\,\mathrm{km\,s^{-1}}$ at $r_0 = 1.4\,\mathrm{kpc}$, is quickly decelerated by gravity and by the sweeping up of matter, leaves the $\sim 15\,\mathrm{kpc}$ galaxy at $\sim 200\,\mathrm{km\,s^{-1}}$ with about 6 times its initial mass (see the thin, solid line). Outside of the galaxy, the same two factors continue to decelerate the wind (see panels 2 and 3), though now the wind ram pressure is also important, imparting enough force to keep the shell at roughly constant velocity out to several hundred kpc. In this example, the wind coasts for a long time, eventually stopping after running into a nearby mass concentration at $\sim 600\,\mathrm{kpc}$ after $\sim 3\,\mathrm{Gyr}$.

The winds in the fiducial model enrich the ICM little, bringing the cluster metallicity to $\sim 0.04\,Z_\odot$, not much more than dynamics alone (see Table 6 and Figure 5). Because the overall metal ejection fraction for winds is about 50% higher than for dynamics alone, this indicates that the cluster environment is suppressing wind escape. More massive groups/clusters are enriched to a rather uniform level, whereas cooler groups show a large scatter in their metallicity. This scatter, which may or may not be supported by observations (see § 3), contrasts with the more uniform enrichment by radiation-pressure ejection (as discussed in § 7 below) and persists even in models in which the metal ejection efficiency is much higher (as in the 'W144max' model described below).

The first row of Table 7 shows $z = 3$ results for the fiducial model using the 128^3 run. Here, galaxies have lost nearly half of their metals, enriching the $\delta = 1$ IGM to a mean metallicity of 1% solar, somewhat higher than the high end of the observed metallicity of the Lyα absorbers of similar or greater density (see Fig. 5).[19] Relative to $z = 0$, the greater escape fraction of metals occurs because the galaxy mass spectrum is shifted toward smaller mass galaxies at high redshift; galactic escape velocities thus become small compared to the fiducial ('W') model's typical outflow velocity. As discussed in Aguirre et al. (2001b), we find that the enrichment of low-density regions is limited primarily by the time available for the shells to propagate into the IGM.

The dependence of the metal escape efficiency on galaxy mass leads to a slightly steeper stellar M-Z relation than does dynamical removal alone, as is evident in Figure 3. The second and fourth panels show galaxy stellar and gaseous metallicity for the fiducial wind model, and the enhanced M-Z relation that wind ejection induces on the galaxies. We see a similar but stronger effect in the $z = 3$ galaxy metallicities of the 'W128' run (not plotted), but there the M-Z relation is evident mainly in the enhanced metallicity of $\gtrsim 10^{10}\,M_\odot$ galaxies where the escape speed approaches the assumed wind velocity.

As in the case of dynamical removal, we have checked some numerical details of the calculation using a number of additional models. First, we have verified that using roughly half or twice as many simulation outputs changes all results insignificantly (i.e. at a similar level as for the same test in the dynamics-only prescription; see Table 5 and Fig. 2). We have checked that all the results are similarly insensitive to the time step used in the integration, the radius over which we average when integrating (as long as it is not large), and the details of the stalling criterion for the shell. The accuracy of the radial integration itself has been checked by propagating shells with all forces except gravity turned off; comparing the shell velocity (computed via integration) to the wind velocity (computed using energy conservation as per Eq. 7) tests the integration accuracy.

A few more numerical details make small but noticeable differences in our results. Halving or doubling the galaxy mass contained within the initial shell radius changes the results of our fiducial model only slightly (at worst by a factor of two in mean metallicity at the lowest densities). The difference between $r_{\rm stall}$ and $h_{\rm wind}$, which adjusts for

[19] Recall that the *mean* metallicity is not necessarily comparable to the observed metallicities if the enrichment is non-uniform; see § 23 and Aguirre et al. (2001b) for discussion.

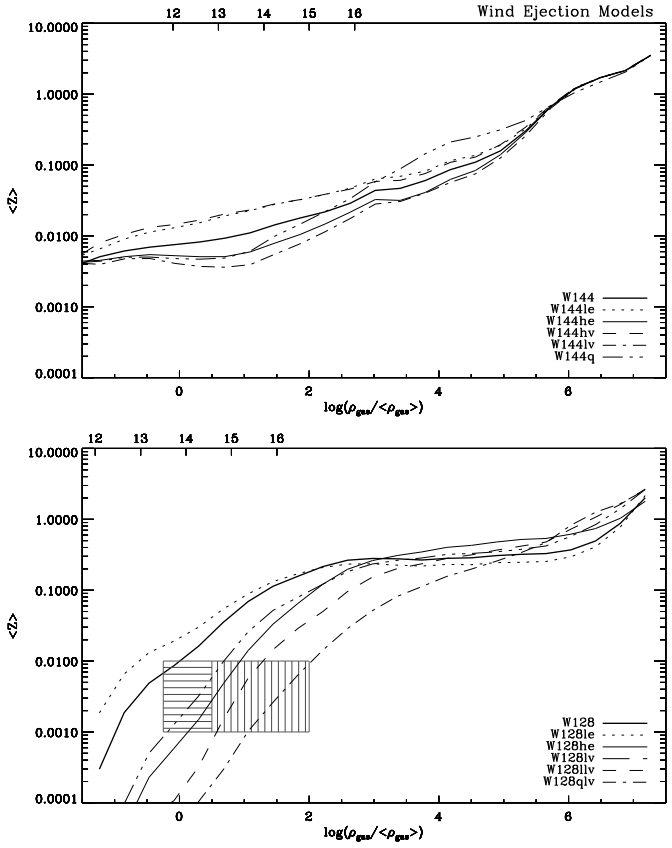

FIG. 6.— Enrichment of the IGM for wind ejection of metals for several wind models (see Table 6) at $z = 0$ (top panel) and at $z = 3$ (bottom panel). Plotted quantities are as in the top panel of Fig 2.

unphysical movement of metals, turns out to have little effect; all results of both the 'W128' and the 'W144' models are changed by $< 10\%$ if this adjustment is removed. A third numerical issue, raised in § 2.2, is that while we calculate the SFR by dividing the stellar mass formed in a galaxy between time $t_{\rm p}$ and $t_{\rm c}$ by $t_{\rm c} - t_{\rm p}$, we assume that this SFR applies for the entire shell propagation time, which may exceed $t_{\rm c} - t_{\rm p}$. Since the SFRs we compute are smooth (i.e. don't depend on short episodes of star-formation) they should vary on roughly the Hubble time. We have run trials in which the wind is turned off entirely a Hubble time after its launch, and find unimportant changes in the results. This insensitivity would also extend to episodic star formation, as long as the episodes are spaced more frequently than the timescale for the wind to decelerate (so that it does not stall between episodes).

A final numerical detail is the number of angles we use, N_a. As described in § 2.2, we choose N_a to ensure ~ 16 gas particles per angle in the galaxy so that the spacing between successive particles in radius is smaller than the scale over which the physical properties of the shell change. This typically results in 2-32 angles per galaxy. Using the 144^3 and 128^3 simulations, we have run trials using 16, 32, 64 and 128 particles per angle. The results are changed very little, indicating that enrichment is quite similar whether we use ~ 2 or $\sim 16 - 32$ angles per galaxy. This insensitivity is probably due to the fairly spheroidal shape of galaxies and their halos in the simulations, and to the fact that winds tend to be either confined, or escape to large radii where the distribution radius is limited primarily by the time constraint. Thus it seems that our results are not significantly affected by lack of angular resolution.

6.2. *Other Wind Models*

Having examined the fiducial model, we now turn to a set of models in which the simulation parameters have been varied. In analyzing these variations we may divide their effects on metal distribution into three aspects. First, the yield y_*, when combined with the simulation's star-formation efficiency, determines the *total* metal content in the simulation volume and the rough normalization of the $M - Z$ relation. Second, $v_{\rm out}^{\rm fid}$, $\rm SFR_{crit}$, $\epsilon_{\rm ent}$, χ and $Y_{\rm ej}$ determine the fraction of metals that escape into the IGM; $Y_{\rm ej}$ controls this directly, whereas the other three control whether outflows occur, whether they are strong enough to escape the galaxies and whether the metals get far enough away from the galaxy so that they do not fall back. These parameters, therefore, directly affect the ratios $f_{\rm IGM}$ and $\langle Z_{\rm cl}\rangle/\langle Z_{\rm gal}\rangle$, as well as affecting the M-Z relation and the level of enrichment of the IGM. Third, $v_{\rm out}^{\rm fid}$, $\dot{m}_{\rm out}/\Omega_{\rm out}$ and $\epsilon_{\rm ent}$ affect how *far* metals travel from their progenitor galaxies; this is most strongly reflected in $\langle Z_{\delta=1}\rangle/\langle Z_{\delta=100}\rangle$ or $\langle Z_{\delta=1}\rangle/\langle Z_{\rm cl}\rangle$, and in the slope of the curves in Figs. 5 and 6.

The effects of changing y_* are clear; the output metallicities of the IGM and galaxies are all proportional to this parameter. Comparison of the M-Z relation of well-resolved simulation galaxies to the observed relation (see Figure 3) indicates $y_* \sim 1$ is appropriate, and values differing from this by more than a factor of ~ 2 could not account for the metallicity of observed galaxies unless $f_{\rm ej} \gtrsim 1/2$.

The effects of changing the parameters $v_{\rm out}^{\rm fid}$, $\rm SFR_{crit}$, $\epsilon_{\rm ent}$ and χ are a bit more complicated and we describe such variations each in turn.

As discussed in § 2.2, superwinds in nearby starburst galaxies appear to be characterized by outflow velocities of $\sim 600\,{\rm km\,s^{-1}}$, but it may be that faster or slower wind velocities better capture the real effect of winds. Models 'lv' and 'hv' (see Figure 6 and Tables 6 and 7) assume wind velocities of $300 \pm 100\,{\rm km\,s^{-1}}$ and $1000 \pm 200\,{\rm km\,s^{-1}}$, respectively. The high velocity model exhibits the features one would expect: more metals escape because the outflows are less easily confined to small radii, and metals travel farther from their progenitor galaxies. Also, the M-Z relation becomes somewhat stronger (the mass threshold above which galaxies tend to retain their metals increases). Both trends are reversed in the low velocity model. Interestingly, the 'W144lv' model shows that some metals reach very low-density regions quite well even if the outflow velocities only drive metals to $\lesssim 100\,{\rm kpc}$. At $z = 3$ in the high resolution simulations the results are similar. IGM enrichment is quite high for the 'W128hv' model, and the enrichment would be far higher if not for the time constraint. This is not surprising since the model assumes $1000\,{\rm km\,s^{-1}}$ winds flowing from dwarf galaxies; it is not clear that such winds could be sustained for long without a catastrophic effect on their hosts. Note, however, that the value of $\rm SFR_{crit}$ is such that the galaxies only drive strong winds early on; thus galaxies cannot eject all of their metals. The 'W128lv' model is interesting for it shows that even low velocity winds can enrich the $\delta = 1$

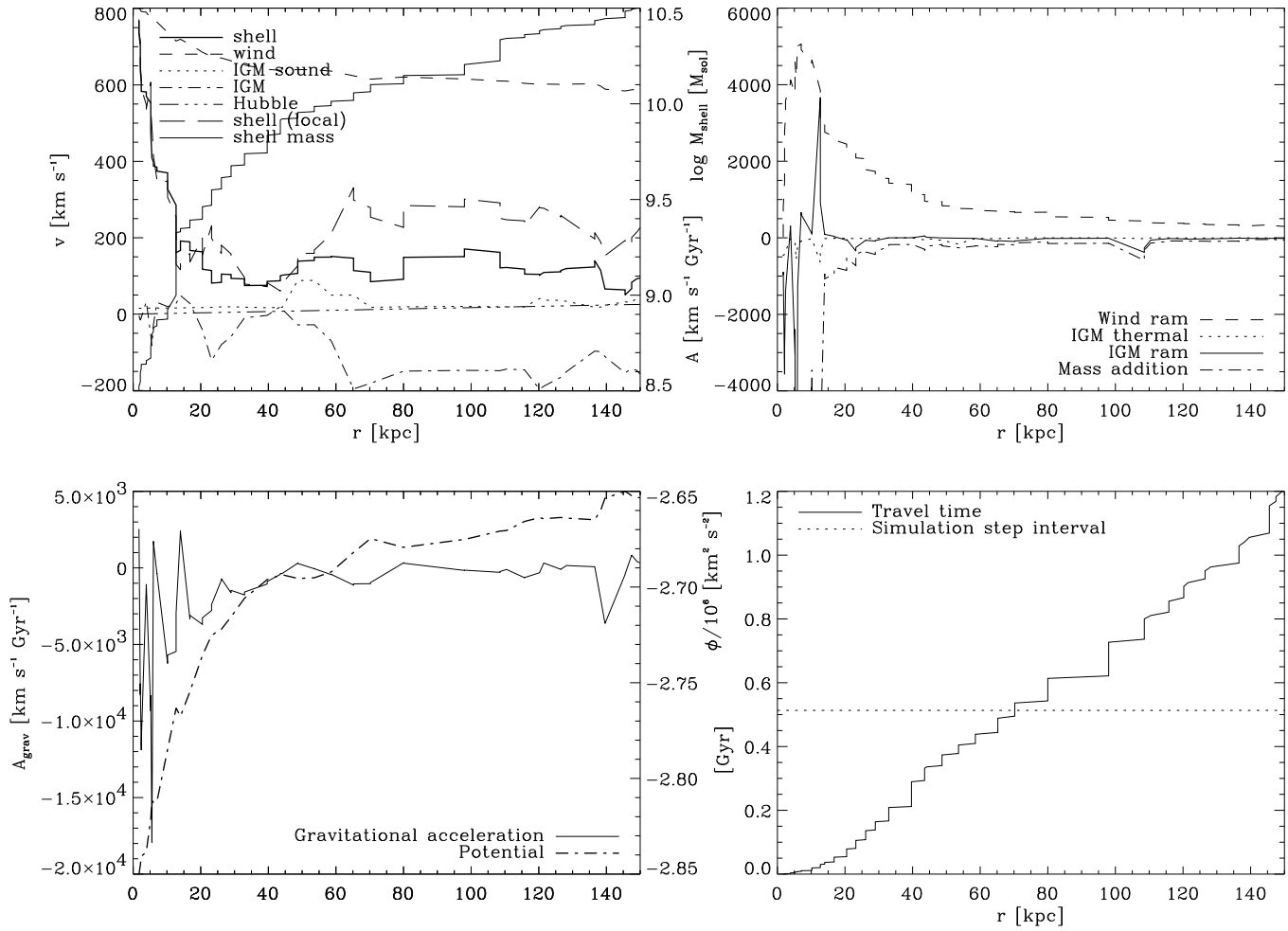

FIG. 7.— Sample for shell propagation at $z = 1.5$, for a shell with initial velocity of $\sim 800\,\mathrm{km\,s^{-1}}$ at initial radius 5.6 kpc in a galaxy of baryonic mass $1.3 \times 10^{11}\,\mathrm{M}_\odot$. **Panel 1:** physical radial velocities (with respect to the galaxy center where appropriate) of the shell, the outflowing wind, the Hubble flow, and the IGM. We give also the local sound speed of the IGM, and the shell velocity in the frame of the ambient gas, as well as the mass of the shell (right axis). **Panel 2:** acceleration of the shell due to the ram pressure of the IGM, the ram pressure of the wind, the thermal pressure of the IGM, and the acceleration due to the addition of mass to the shell (i.e. the term $(v/m)(dm/dt)$ where v and m are the velocity and mass of the shell). **Panel 3:** Acceleration due to gravity (left axis) and gravitational potential (right axis). **Panel 4:** Elapsed time since launch at initial radius. The dotted line indicates the time corresponding to the next simulation output used.

IGM to $1/1000\,Z_\odot$ (assuming that the overestimation of the SFR and Ω_* by the simulation is not too severe; see § 4). We have also tested even lower outflow velocities at high z; model 'W128llv' assumes outflow velocities of $100 \pm 50\,\mathrm{km\,s^{-1}}$. Even this model enriches the IGM at $\delta > 10$ to a *mean* level of $\gtrsim 1/1000\,Z_\odot$.

As discussed in § 2.2, galaxies with SFR/(area) $\lesssim 0.1\,\mathrm{M_\odot\,yr^{-1}\,kpc^{-2}}$ do not seem to drive observable superwinds, whereas starburst galaxies that *do* drive such winds can have much higher areal SFRs. But since we cannot formulate a rigorous criterion for which galaxies in our simulations are driving winds, it is useful to check how strongly the enrichment predictions depend on $\mathrm{SFR_{crit}}$. Models 'W144lcrit' and 'W144hcrit' (not plotted) reveal that halving or doubling $\mathrm{SFR_{crit}}$ changes the results in a predictable way. For $\mathrm{SFR_{crit}} = 0.05$, all galaxies at $z = 2$ drive outflows, as do a small fraction of $z = 0$ galaxies. The ejection efficiency is significantly increased, as is $\langle Z_{\delta=1}\rangle$; there is a somewhat smaller effect on the IGM metallicity. Further decreasing the critical SFR would have only a small effect. These trends are roughly reversed when $\mathrm{SFR_{crit}}$ is doubled, although in this case yet higher values would lead to progressively more suppression of winds.

An important uncertainty in our assumptions is the entrainment fraction ϵ_{ent}, introduced to account for the fact that an expanding wind-driven shell almost certainly fragments and may either leave a large fraction of itself behind or significantly reduce its covering factor, or, even if fragmentation is not severe, may not sweep up all of the ambient medium if the gas is clumped. In principal this parameter could be deduced from numerical simulations, but current simulations do not follow the shell far enough into the IGM or resolve small-scale structure in the gas well enough to do this. We have tried values of ϵ_{ent} of 1%, 10% and 100% in model 'le', the fiducial model, and 'he' respectively. These reveal that the entrainment fraction is quite important (see Figure 6 and Tables 6, 7), especially in the lower-mass galaxies (the high mass galaxies tend to retain their winds gravitationally). The differences are particularly large in the enrichment of the low-density IGM. As in the case of the wind velocity, this sensitivity is actually useful, as it could be used to constrain the properties of winds given the observed enrichment of the IGM (if winds are assumed to be responsible).

Another parameter that is somewhat uncertain is the wind efficiency χ that fixes the constant of proportionality between the wind energy and the SFR. We have calibrated χ to reproduce the approximate observed mass outflow rates. Models 'lχ' and 'hχ' show the effect of changing this efficiency by a factor of two. The effect is significant, showing that continual driving by the wind is important in the shell's propagation. The importance of χ decreases with increasing ϵ_{ent} (as the shell propagation becomes dominated by conservation of the initial shell momentum).

Two final parameters that might be varied (and for which *a priori* values are hard to justify) are α (controlling the steepness of the radial profile of metal distribution) and β (the sharpness of the energy attenuation below $\mathrm{SFR_{crit}}$). Trials with $\alpha = 1, 2, 3$ and 4 have at most $\sim 20\%$ differences in the output quantities listed in Table 6. Different values of β give important differences in the results, but entirely predictable ones. For $\beta = 0$ the results are similar to the 'Q' model described below (i.e. they simulate $\mathrm{SFR_{crit}} = 0$). Choosing larger values of β has no effect for small $\mathrm{SFR_{crit}}$, a drastic effect if all of the galaxies have $\mathrm{SFR} < \mathrm{SFR_{crit}}$, and an effect similar to raising $\mathrm{SFR_{crit}}$ itself for intermediate values.

In summary, we find that the fraction of metals that escape galaxies, expressed as f_{IGM} or $\langle Z_{\mathrm{cl}}\rangle/\langle Z_{\mathrm{gal}}\rangle$, is fairly sensitive to the assumed outflow velocity and to the entrainment fraction (varies by a factor of 2-3 within our assumed range), is slightly less sensitive to the critical SFR/(area) and wind efficiency (varies by less than a factor of 2), roughly scales with Y_{ej}, and is insensitive to other parameters such as α and β. Very similarly, the enrichment of low-density regions, which requires metals to travel farther from their progenitor galaxies, is also sensitive to $v_{\mathrm{out}}^{\mathrm{fid}}$ and ϵ_{ent} ($\langle Z_{\delta=1}\rangle$ varies by a factor of up to ~ 10). Low-density enrichment is somewhat less sensitive to the assumed critical SFR and wind efficiency, again roughly scaling with Y_{ej}, and is not sensitive to α or β. Cosmologically-averaged metal mass is determined by y_* but can be constrained strongly by comparing the calculations to the observed M-Z relation and cluster metallicities.

After varying many of the parameters individually, we have also varied combinations of parameters to model various physically distinct possibilities. First, we have performed trials with $\epsilon_* = 0.004/\Omega_*^{\mathrm{sim}}(z = 0) = 0.36$; this is equivalent to dividing $\mathrm{SFR_{crit}}$, and multiplying χ and y_*, by the same value. As described in § 2.4, ϵ_* is introduced to account for possible differences between the simulated and observed SFR, mass function and Ω_* of galaxies. Setting a low ϵ_* accurately mimics an IMF in which most mass goes into low-mass stars and brown dwarfs, and somewhat less reliably adjusts for over-efficient star formation in the simulations. The 'lsfr' models show significantly less ejection and a smaller enrichment of the IGM. The smaller ejection fraction is largely due to the effectively larger $\mathrm{SFR_{crit}}$. Winds reach smaller radii, due to the lower effective value of χ. The very low metallicity of the low density IGM is a product of the lowered y_* and the lower ejection efficiency. The former effect is realistic if Ω_*/Ω_b is significantly overestimated by the simulations. However, if we do assume a steep IMF so that many low-mass objects are present, we see that $y_* > 1$ would be required if galaxies are to have reasonable metallicities, and this would tend to cancel the effect.

As pointed out in §2.2, we have formulated our model to simulate powerful winds from galaxies with the highest SFRs. But even galaxies that are *not* undergoing violent star formation may drive winds (c.f. § 2.2), though these must have $\chi \lesssim 1$ most of the time, or they would disassemble the entire galaxy over time (the mass outflow rate given by Eq. 4 would always be larger than the SFR). The 'q' and 'qlv' models were chosen to represent such winds; $\mathrm{SFR_{crit}}$ is set low enough so that almost all galaxies drive winds. The wind efficiency χ is 1/10th its fiducial value, and $Y_{\mathrm{ej}} = 0.5$. At low-z and from massive galaxies, IGM enrichment in model 'W144q' is almost as effective as in model 'W144', both because the wind stopping radius depends fairly weakly on χ, and the larger fraction of galaxies driving winds compensates for the less effective ejection. At high-z the 'W128q' model enriched significantly less than the fiducial model; this occurs because most galaxies

at $z > 3$ are driving winds even for the fiducial value of $\mathrm{SFR_{crit}}$. The 'qlv' model assumes also that the winds are relatively slow-moving. The enrichment in this model is very weak at both high and low z, thus if 'quiescent' winds are to enrich the IGM significantly, they must have fairly high velocity.

Given the assumption that wind speed does not depend on galaxy mass, low mass galaxies (mostly unresolved by the 144^3 simulation) should eject metals most efficiently. Thus we expect our 144^3 simulations to underpredict the IGM enrichment due to winds. Nevertheless it is interesting that neither the fiducial model nor any of its minor variants can account for the metal enrichment of groups/clusters. Because we resolve most of the observed $z = 0$ mass function, this indicates that something other than winds provides the bulk of the enrichment, or that the enrichment happens at fairly high redshift (where the mass function shifts to lower mass galaxies not resolved by the 144^3 simulation), or that winds are described by parameters somewhat different than those we have assumed. To make this point more robust, we have generated a 'maximal' model, 'W144max', which combines a high wind velocity, high wind efficiency, low entrainment fraction and low critical SFR. While galaxies in this model eject $\sim 20\%$ of their metals, the enrichment of clusters is still only about 1/10th solar, several times smaller than observed. Moreover, this is achieved at the cost of a mass-metallicity relation significantly steeper than that observed. In fact, it does not appear possible to fit both the M-Z relation and the cluster metallicity for any set of parameters (i.e. without modifying the method). Because of the low resolution of our $z = 0$ simulation it is premature to draw strong implications for the enrichment of clusters, but we hope to return to this topic in a future study.

An interesting physical effect we can examine with our calculations is the effect of winds on *dynamical* enrichment: if metals are moved into galaxy halos, it seems likely that they will be more easily removed by dynamical processes. This effect has been seen in detailed simulations by Murakami & Babul (1999) of galactic winds in clusters, and discussed in the context of 'general' IGM enrichment by Ferrara et al. (2000). To investigate this effect we have run wind models in the 128^3 and 144^3 simulations with wind velocities of $300 \pm 100\,\mathrm{km\,s^{-1}}$ and $1000 \pm 200\,\mathrm{km\,s^{-1}}$, respectively. In the first, we generate metals only at $z = 5$, and examine their distribution at $3 \le z \le 5$. In the second, we generate metals only at $z = 2$, and examine their distribution at $0 \le z \le 2$. The results are shown in Fig. 8, with the 128^3 runs on the left and the 144^3 on the right. The top panels shown median metallicities; mean metallicities are given in the bottom panels. The right panels show that at low z the effect exists; some metals deposited at $\delta \gg 100$ find themselves at $\delta \lesssim 100$ at $z = 0$. But the effect is slight, and is strongest (particularly as evinced by the median metallicities) at $\delta \sim 100$, suggesting that it may be happening primarily in groups and clusters. Indeed the left panels show that between $z = 5$ and $z = 3$ metals tend to migrate from low- to high-density regions (the metals which go 'missing' from the plots are those absorbed by stars). Thus it seems that in the 'general' IGM, dynamics tend to move metals from moderate density regions into galaxies and other higher-density regions, rather than distributing them more widely into low-density regions.

6.3. *Summary and Discussion*

In summary, we find that many physically distinct 'types' of winds can enrich the IGM to comparable levels. For example, quiescent winds (weak winds from all galaxies) can enrich the IGM at all densities to a similar level (within a factor of two) as winds with very strong outflows from only the galaxies with the very highest SFRs. The predictions are, however, different enough (e.g., in the M-Z relation) that with refined simulations and better observational data our calculations could be used to constrain the physical models of winds themselves.

While the emphasis of this paper is methodology, we can draw some general conclusions regarding wind enrichment of the IGM using our calculation. We repeat that we have *not* shown that winds can develop in any particular type of galaxy (as in e.g., Mac Low & Ferrara [1999] or Strickland & Stevens [2000]). Instead, we assume the wind properties based on observations, amalgamating the physical criteria for a wind into the methodological criterion of a high enough areal SFR. Under this assumption, galaxies can lose a significant fraction of their metals to the IGM. Averaged over all galaxies, we find that typically 5-50% of metals are expelled into the IGM, and that the fraction is highly degenerate in the assumed parameters.

Our calculations indicate that galactic winds can enrich even the low-density regions of the IGM quite effectively. At $z = 3$, winds escape to large radii, and the ensuing enrichment is sufficient to roughly account for the metallicity seen in low-density Lyα absorbers (see Aguirre et al. 2001b for more discussion). Enrichment of the IGM becomes progressively higher, and spreads to progressively lower density regions of the IGM, as redshift decreases; this is in agreement with the findings of Cen & Ostriker (1999). At $z = 0$, we predict that even quite underdense regions of the IGM are enriched to a mean metallicity of $Z \gtrsim 0.005\,Z_\odot$ unless the parameters are pushed to unreasonable values.

The main implication we can draw for the enrichment of cluster gas is that large galaxies can enrich the gas to $\sim 1/10$ of its observed metallicity given our fiducial model assumptions about the wind properties. (Some of this enrichment is direct, and some probably occurs because metals are moved into galactic halos where they are more easily removed by dynamical processes.) This is probably an underestimate of the overall importance of winds to cluster enrichment because we cannot address the importance of low-mass galaxies at high redshift, which would eject metals more efficiently. If winds are to account for the metals in clusters, we find that the enrichment must happen at relatively high redshift, or that one of our assumptions regarding winds must be modified.

Our simulations also make predictions about the properties of galaxies. While our range in galaxy masses is too small for a conclusive comparison, we find that the M-Z relation is nevertheless a good way to break the degeneracy between our parameters – especially that between outflow speed and wind efficiency. While there seems to be an M-Z relation in observed bright ($M_B \lesssim -21$) galaxies, we have difficulty reproducing this relation. Several effects may contribute to this difficulty. First, our assump-

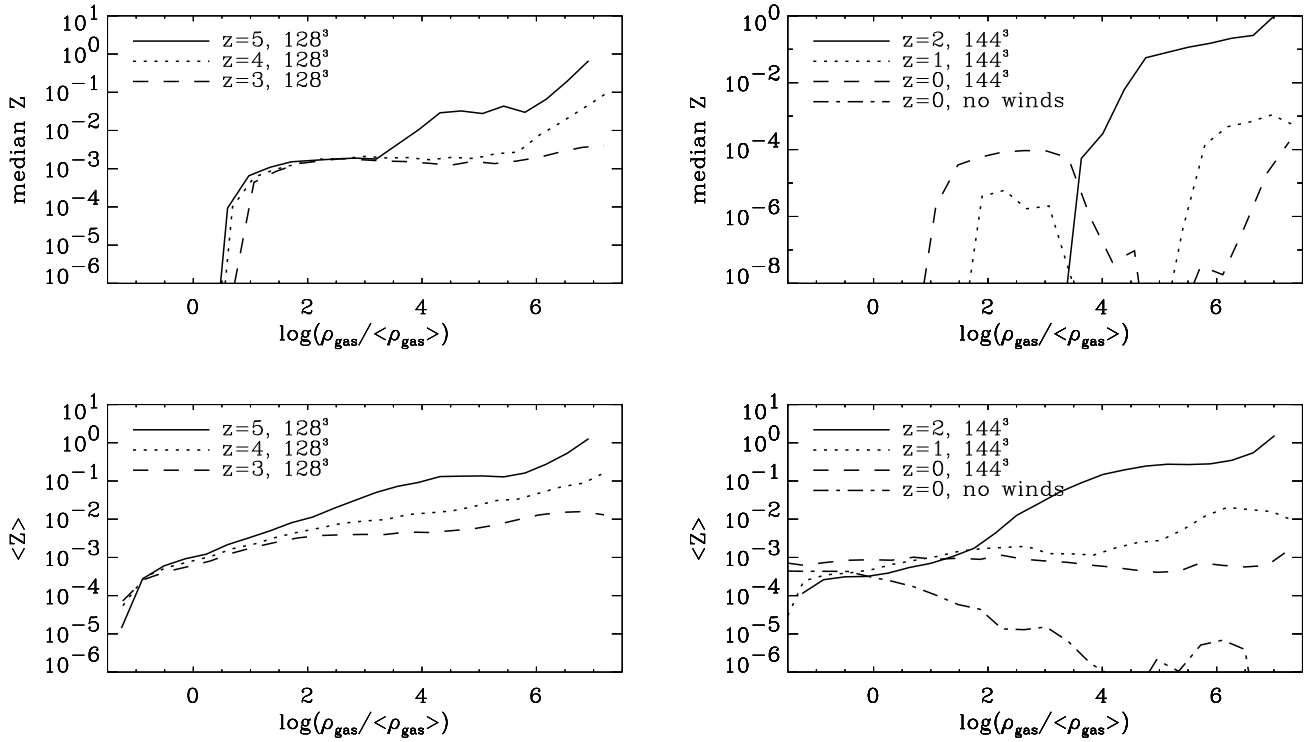

FIG. 8.— Movement of metals by gas processes after their distribution near galaxies by winds. Only the timestep at $z = 5$ (left panels) or at $z = 2$ (right panels) was enriched. The median (top panels) and mean (bottom panels) metallicity (vs. density) at lower redshifts is plotted, showing the flows of enriched gas between regions of different density. Metals which seem to 'disappear' with decreasing redshift are those incorporated into stars. We also plot the $z = 0$ results for local enrichment (no winds) at $z = 2$ (right panels). This line is missing from the top right panel because the median gas metallicity is everywhere zero.

tions that all galaxy types have the same outflow velocity may be flawed; but experimentation reveals that we would have to change this assumption drastically to alter the high-mass M-Z relation, partially because the highest mass galaxies tend to be in clusters where the ICM suppresses their winds. Second, the brightest galaxies may be too extended for our method to treat well (i.e. the winds are stopped inside and by the galaxy itself). Third, the 'average' metallicity determined by observations may include fewer of the outlying, low-metallicity stars than in the simulations. Finally, it may be that something besides wind ejection causes the observed M-Z relation in massive galaxies.

The results reported in this section point to a few general conclusions regarding our methodology. First, like semi-analytic theories of galaxy formation, the method employs a number of parameters that strongly affect the calculation predictions and that cannot be ascribed definite values using observational data. This limits the number of specific general conclusions we can draw. Nevertheless, the method is excellent for generating predictions *given* a specific model (e.g., the model based on locally observed starburst-driven superwinds). Further studies, either observational or theoretical, producing more robust physical models of winds will generate correspondingly more robust predictions of the cosmic metal distribution using our method.

7. MODELS AND RESULTS FOR DUST EJECTION

7.1. *Fiducial Dust Model*

Radiation-pressure driven efflux of dust from galaxies provides an interesting alternative to galactic winds to pollute the IGM with metals. A number of studies have pointed out that typical spiral galaxies could eject a significant amount of their dust *if* the dust can decouple from bound gas and magnetic fields (e.g., Chiao & Wickramasinghe 1972; Ferrara et al. 1990; Shustov & Vibe 1995; Davies et al. 1998; Simonsen & Hannestad 1999). Our method does not directly address the question of whether dust can decouple but *can* yield a reasonable estimate of the equilibrium radius of dust for galaxies with properties given by the simulations. If dust can escape the inner galaxy there should be no obstacle to its reaching the equilibrium radius, provided it can do so in a short enough time. We can, therefore, give plausible estimates of the radii to which dust grains might be ejected by galaxies of various masses, ages and types, at various redshifts, and track the distribution of metals after they are deposited, even if they only reach the halos of galaxies.

Our fiducial dust-ejection model, labeled 'P144' and 'P128' in Table 8 and in the figures, assumes graphite grains with $Q_{\rm pr}/a\rho = 19$ (see eq. 10); this is the maximum absorption efficiency from graphite grains subject to a 12,000 K blackbody spectrum. We assume a Scalo IMF in calculating the stellar luminosities, and a dust correction depending on metallicity, adjusted so that the integrated background light has equal parts in FIR and UV-optical-NIR. We assume that half of each galaxy's metals are distributed non-locally ($Y_{\rm ej} = 0.5$), which is an upper limit since only about half of a typical galaxy's metal mass can be in dust. (Also, the connection between the metal outflow rate and the SFR is much less clear for dust ejection than for supernova winds.)

The results of the fiducial model are given in Table 8 and Figs. 3, 9, 10, and 11. The table and the first two figures give the same quantities that were presented for winds, while the last two figures give details about the ejection from individual galaxies.

Under our assumptions, dust ejection is fairly efficient. In the 144^3 simulation, $z = 0$ galaxies have lost 16% of their metals, meaning that 32% of the dust that we assume *can* escape actually does escape, with the rest being retained either because it falls back into galaxies or because the galaxies have insufficient light/mass ratios to eject it. The ejected dust enriches the intracluster gas to $\sim 1/5\,Z_\odot$, and the $z = 0$ IGM at mean density is enriched to $0.02\,Z_\odot$. These values can be roughly linearly scaled to lower values of $Y_{\rm ej}$. Dust ejection at high z pollutes the $\delta = 1$ IGM at $z = 3$ to $\sim 10^{-4}\,Z_\odot$. The values given are for *all* metals (solid and gaseous). Figure 12 also shows the amount of dust converted to gaseous metals by $z = 3$ due to thermal sputtering, in a number of models including the fiducial model. Nonthermal sputtering and dust destruction during ejection would also destroy some dust, so the actual level of observable gaseous metals should lie between the 'gaseous metals+dust' curves and the 'gaseous metals only' curves.

A few aspects of the results for the fiducial model merit attention. First, the enrichment of low-mass groups is much more uniform than in the wind or dynamics-only model (compare figures 2, 5 and 9). For dust ejection, the metallicity of hot gas declines steadily with gas temperature, leveling off for the hottest clusters. For wind ejection – even for runs with $f_{\rm ej} \sim 1/5$ – there is a large scatter in the metallicity of groups. It is currently unclear which of these cases has more observational support. Second, as is evident from Figure 3, the M-Z relation of galaxies is enhanced by dust ejection over the dynamical removal case and is more similar to the observed relation (the gas metallicities match the observations particularly well). The M-Z relation is, however, somewhat different than for winds; although the general trend is similar, there is more scatter of low-mass galaxies into high metallicities, and a somewhat less abrupt drop at masses $M \lesssim 10^{11}\,{\rm M}_\odot$ (especially compared to wind models with a high escape fraction). As in the wind case, the stellar M-Z relation for the most massive galaxies is flatter than observed.

We can investigate the enrichment process in more detail by examining the properties of the galaxies driving the dust outflows. Figures 10 and 11 show the relations between galaxy mass M, metallicity Z, mass-to-light ratios M/L_B and $M/L_{\rm bol}$, and maximum radius of dust ejection $h^{\rm dust}$. Interestingly, at $z \gtrsim 1$, fairly large galaxies drive dust to the largest radii, whereas at $z \lesssim 1$, dust ejection is most efficient in the smallest and the largest galaxies (see panel 4 of both figures). This occurs because large galaxies have a relatively larger ratio of stars to gas and dark matter. At lower redshifts, this effect is overwhelmed in the smallest galaxies by the dust correction (which increases M/L more in large galaxies; see panels 2 and 5), and by the tendency of smaller galaxies to be younger.

At high z, graphite dust can be driven to $\sim 1\,{\rm Mpc}$ by at least some galaxies, whereas at low z galaxies can drive dust only to a few hundred kpc. The $z = 0$ galaxies have typical bolometric (dust corrected) M/L values

Table 6
Wind Models, 144^3 simulation

Model	Variation	$f_{\rm IGM}$	$\langle Z_{\delta=1}\rangle$	$\langle Z_{\delta=100}\rangle$	$\langle Z_{\rm cl}\rangle$	$\langle Z_{\rm gal}\rangle$
W144	none	0.057	0.008	0.019	0.037	0.83
W144he	$\epsilon_{\rm ent} = 1$	0.044	0.0052	0.012	0.031	0.84
W144le	$\epsilon_{\rm ent} = 0.01$	0.086	0.013	0.035	0.054	0.79
W144lsfr	$\epsilon_* = 0.355$	0.035	0.0015	0.0025	0.0070	0.31
$W144_{np32}$	32 galactic gas particles/angle	0.056	0.0073	0.019	0.036	0.83
$W144_{np128}$	128 galactic gas particles/angle	0.056	0.0073	0.018	0.036	0.83
W144hv	$v_{\rm out}^{\rm fid} = 1000\,{\rm km\,s^{-1}}$	0.088	0.015	0.035	0.057	0.79
W144lv	$v_{\rm out}^{\rm fid} = 300\,{\rm km\,s^{-1}}$	0.038	0.0040	0.0091	0.025	0.85
W144hcrit	${\rm SFR_{crit}} = 0.05$	0.039	0.0048	0.0088	0.023	0.86
W144lcrit	${\rm SFR_{crit}} = 0.2$	0.091	0.012	0.039	0.051	0.79
W144hχ	$\chi = 2.0$	0.073	0.011	0.028	0.046	0.81
W144lχ	$\chi = 0.5$	0.047	0.0057	0.014	0.032	0.84
W144max	hv, lcrit, hχ, le	0.22	0.042	0.10	0.12	0.66
W144q	${\rm SFR_{crit}} = 0.001$, $\chi = 0.1$	0.052	0.0048	0.017	0.032	0.83
W144qlv	q+lv	0.036	0.0039	0.0082	0.022	0.85

Note: all results are given at $z = 0$.

Table 7
Wind Models, 128^3 simulation

Model	Variation	$f_{\rm IGM}$	$\langle Z_{\delta=1}\rangle$	$\langle Z_{\delta=100}\rangle$	$\langle Z_{\rm gal}\rangle$
W128	none	0.47	0.01	0.18	0.34
W128he	$\epsilon_{\rm ent} = 1$	0.19	0.00079	0.09	0.52
W128le	$\epsilon_{\rm ent} = 0.01$	0.58	0.022	0.19	0.26
W128lsfr	$\epsilon_* = 0.355$	0.18	0.0017	0.021	0.18
$W128_{np32}$	32 galactic gas particles/angle	0.47	0.0093	0.19	0.33
$W128_{np128}$	128 galactic gas particles/angle	0.54	0.0099	0.23	0.28
W128hv	$v_{\rm out}^{\rm fid} = 1000\,{\rm km\,s^{-1}}$	0.57	0.017	0.20	0.27
W128lv	$v_{\rm out}^{\rm fid} = 300\,{\rm km\,s^{-1}}$	0.22	0.0017	0.098	0.51
W128llv	$v_{\rm out}^{\rm fid} = 100\,{\rm km\,s^{-1}}$	0.086	0.00016	0.038	0.61
W128hcrit	${\rm SFR_{crit}} = 0.05$	0.32	0.0080	0.12	0.40
W128lcrit	${\rm SFR_{crit}} = 0.2$	0.48	0.010	0.19	0.33
W128hχ	$\chi = 2.0$	0.56	0.016	0.21	0.28
W128lχ	$\chi = 0.5$	0.36	0.0056	0.15	0.41
W128q	${\rm SFR_{crit}} = 0.001$, $\chi = 0.1$	0.083	0.00031	0.036	0.63
W128qlv	q+lv	0.033	5.8×10^{-5}	0.010	0.68

Note: all results are given at $z = 3$.

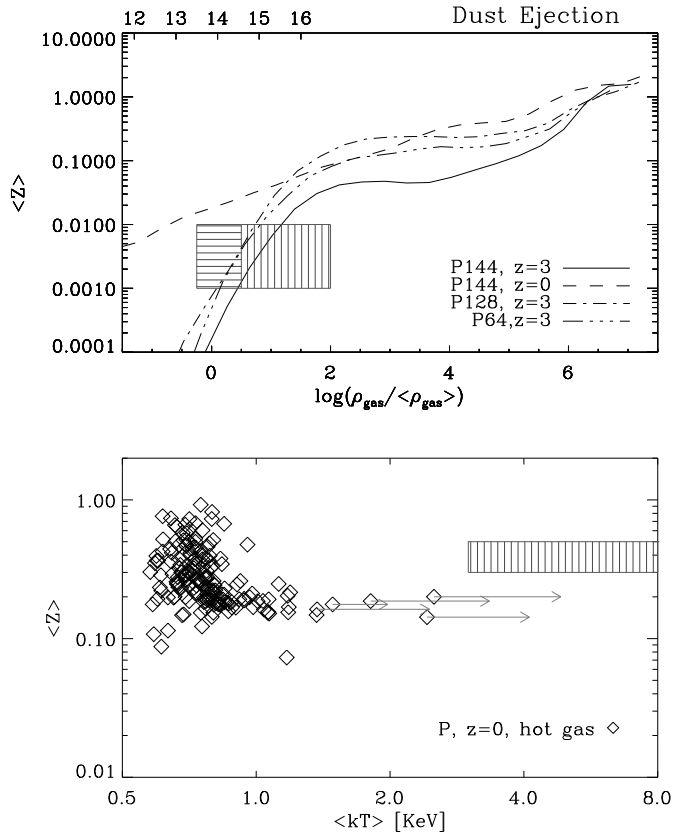

FIG. 9.— Enrichment of the IGM for radiation pressure ejection of dust in the fiducial 'P144' model (see Tables 2 and 8). Plotted quantities are as in Fig 2.

of $\sim 1-5$ and *uncorrected* M/L_B ratios of $\sim 1-4$. Panel 6 of Figure 11 shows the B-band luminosity function of the $z = 0$ simulation galaxies computed using the simple spectral synthesis described in 2.3, and compares it to the 2dF observed luminosity function (dashed line). The simulated luminosity function with no dust correction (light solid line) is a poor fit to the observations. The dark solid line shows the same data with the metallicity-dependent dust correction (given in Eq. 18) used in calculating dust ejection. Applying this correction requires a choice of C_f, where 10^{C_f} (in this context) is the ratio of B-band extinction to UV (1900 $\mathring{A}$) extinction. The curve shown assumes $C_f = -0.5$; with such a choice the simulations can roughly fit the observed luminosity function. The actual relation between UV and blue extinction depends not only on the dust absorption curve but also on the amount and distribution of dust in the galaxy (see, e.g., Charlot & Fall 2000) and is uncertain; but $C_f = -0.5$ is not an unreasonable value, indicating that the dust correction and spectral synthesis methods can probably produce satisfactory (good to within a factor of a few) luminosities for our simulation galaxies.

7.2. *Other Dust Models*

We now investigate the effects of variations in the model parameters. As in the wind models, y_* determines the total simulation metal mass. The amount of metals driven from galaxies depends directly on $Y_{\rm ej}$, less directly on $Q_{\rm pr}/a\rho$, the M/L ratio from stellar synthesis, and the dust correction, and quite weakly on the form of $W_{\rm grp}$; the last four quantities also determine how far the dust travels. In turn, $Q_{\rm pr}/a\rho$ depends primarily on the dust type, M/L values depend on the IMF, and the dust correction depends on the FIR/optical ratio of the extragalactic background light.

The absorption efficiency of dust grains depends mostly on their composition; in this study we have used opacities for both graphite grains and less efficiently absorbing silicate grains. Model 'sil' assumes the latter. Since the maximal $Q_{\rm pr}/a\rho$ is 1/5 that of graphite, ejection is significantly less efficient (see Table 8 and Figure 12). This is important because the majority of dust mass is locked in silicates in most carbon/silicate grain models (e.g., Weingartner & Draine 1999; Duley, Jones & Williams 1989; Mathis & Whiffen 1989). Thus a model in between the fiducial model and the 'sil' model is a more accurate representation of a realistic dust distribution for a two-component model.

We next tried a model with an assumed Salpeter IMF, with $0.1\,{\rm M}_\odot \le M \le 125\,{\rm M}_\odot$. This resulted in somewhat brighter galaxies at $z \gtrsim 0.5$, and somewhat dimmer galaxies at $z \lesssim 0.5$; the overall effect is to slightly enhance dust ejection. The effect on the M-Z relation is also weak. The simulation results are also somewhat sensitive to the choice of the low-mass cutoff in the IMF, as this changes the stellar mass with little effect on the luminosity. For example, starting the Salpeter IMF at $0.2\,{\rm M}_\odot$ rather than $0.1\,{\rm M}_\odot$ would lower M/L by $\approx 24\%$ and the low-mass IMF advocated by Gould, Flynn & Bahcall (1996) would decrease it even more. These uncertainties are, however, unlikely to change M/L by more than a factor of two and are hence contained within the range of variations we try.

The assumed dust correction is more important than the chosen IMF, and comparable in importance to the choice of grain properties. Maintaining the dust correction based on metallicity, we have varied C_f to reproduce a present-day ratio of $1/3 \le F_{\rm FIR}/F_{\rm opt} \le 2$ in the $z = 0$ extragalactic background (where $F_{\rm opt}$ includes UV and NIR light also). The extremes of this range are shown in models 'wcorr' and 'scorr' in Table 8. Although $h^{\rm dust}$ is generally several times higher in the 'wcorr' model than in 'scorr', the enrichment of the low-density IGM is quite similar. This indicates that very low-density IGM regions can be spatially close to high-density metal-forming regions. We also modeled a constant dust correction with $F_{\rm FIR}/F_{\rm opt} = 1$, in model 'ccorr', and a luminosity-dependent dust correction (model 'lcorr'). The results are only slightly different from the fiducial case. As in the other prescriptions, the dust ejection calculations are insensitive to the number of time steps employed.

Ejection of dust by radiation pressure requires that the dust decouple from the gas. Even in the brightest galaxies, radiation pressure cannot overcome the gravitational force on both dust and an associated gas mass more than 100 times as large. We have verified this in our simulations using a trial with $Q_{\rm pr}/a\rho = 0.19$, and no dust correction. The results are nearly identical to the dynamical removal run, indicating that radiation pressure is in this case ineffective even at moving dust into the halos of galaxies.

7.3. *Summary and Discussion*

The fiducial dust ejection model can account for both the low-density IGM metallicity at $z = 3$ and a signifi-

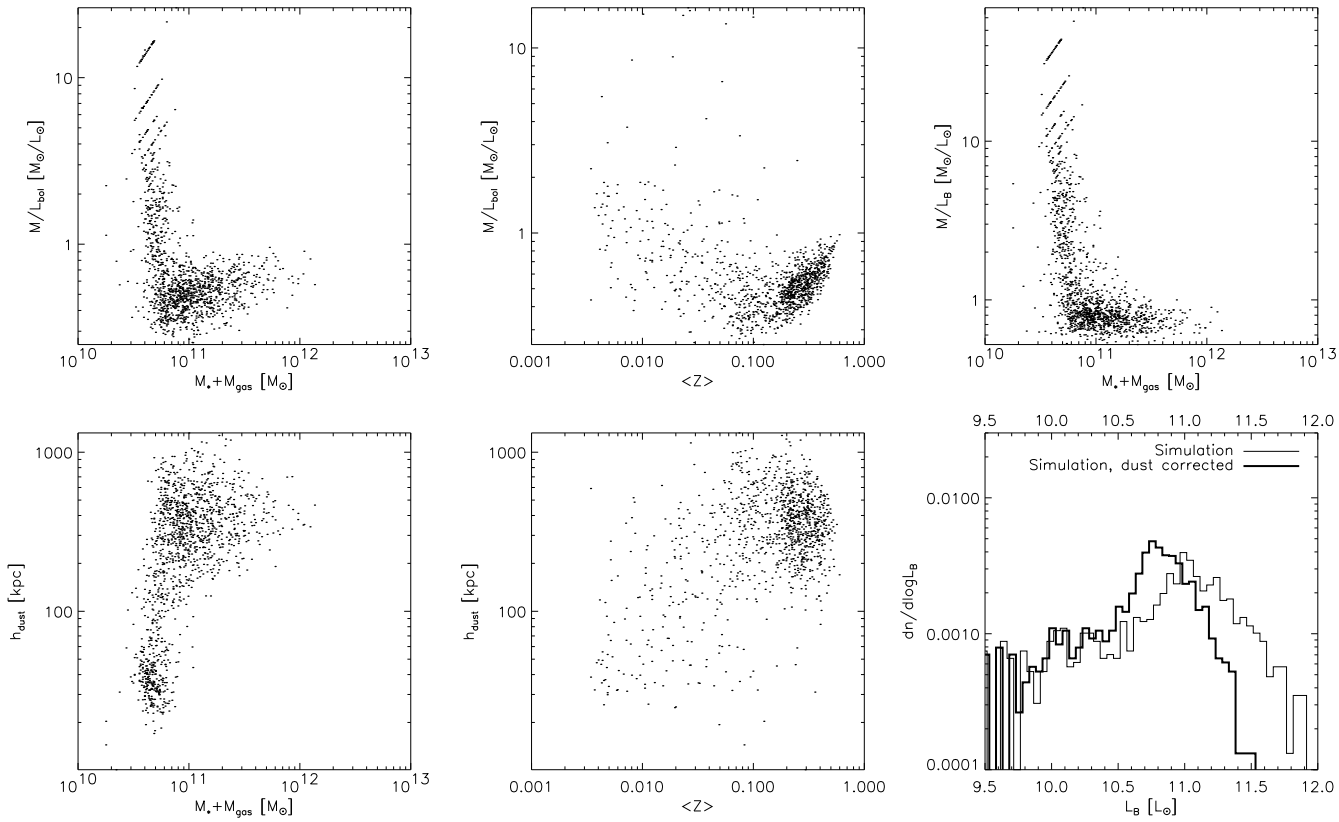

FIG. 10.— Quantities used in dust ejection for the fiducial 'P144' model at $z = 2$. **Panel one:** Bolometric mass/light ratio $M/L_{\rm bol}$ vs. galaxy mass. **Panel two:** $M/L_{\rm bol}$ vs. galaxy average metallicity. **Panel three:** B-band M/L_B vs. galaxy mass. **Panel four:** Maximal dust ejection radius $h^{\rm dust}$ vs. galaxy mass. **Panel five:** $h^{\rm dust}$ vs. mean metallicity. **Panel six:** B-band luminosity function of simulated galaxies, uncorrected for dust (solid, thin) and corrected for dust using metallicity (solid, thick). Top axis gives B-band magnitude.

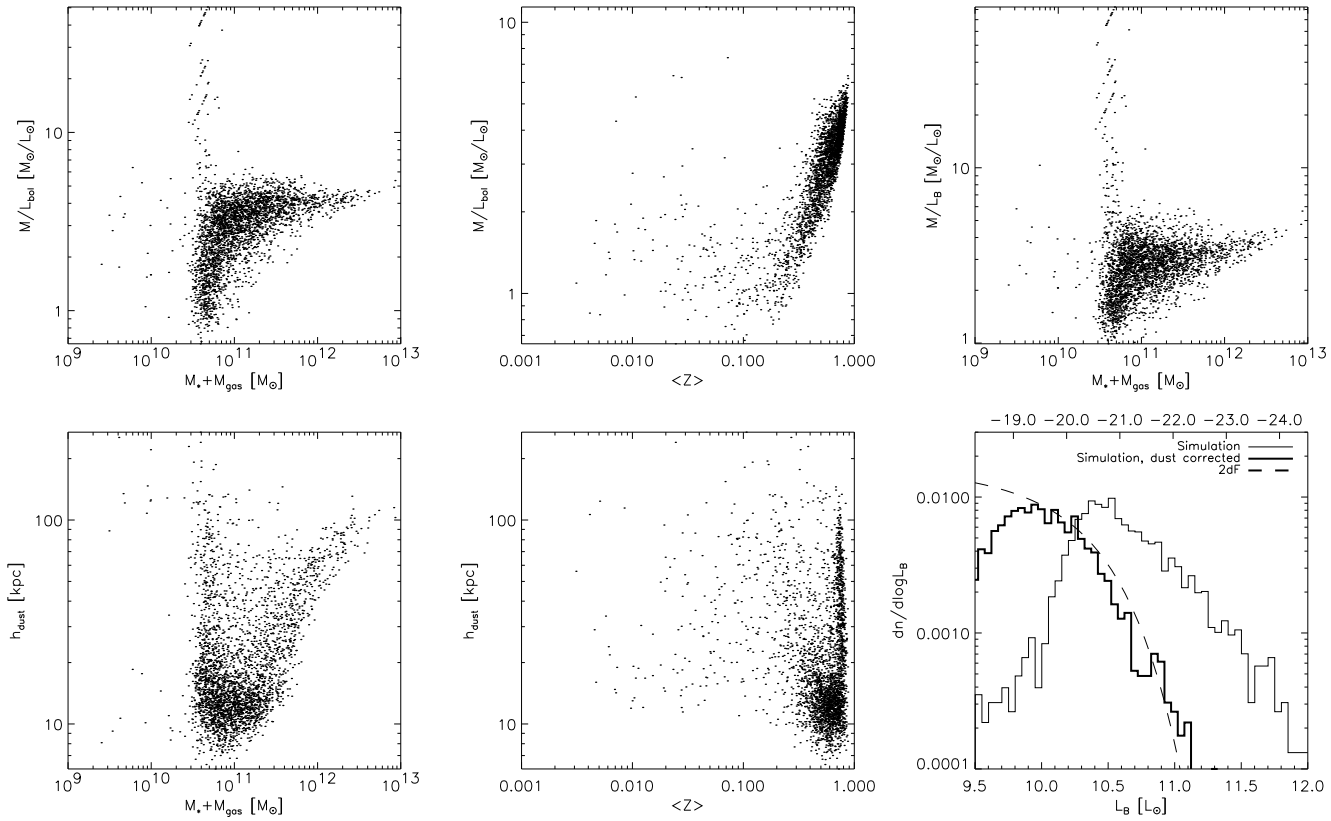

FIG. 11.— Quantities used in dust ejection for the fiducial 'P144' model at $z = 0$. Plotted quantities are as in Figure 11, except that we include the observed 2dF B-band luminosity function in panel 6 for comparison with the simulation.

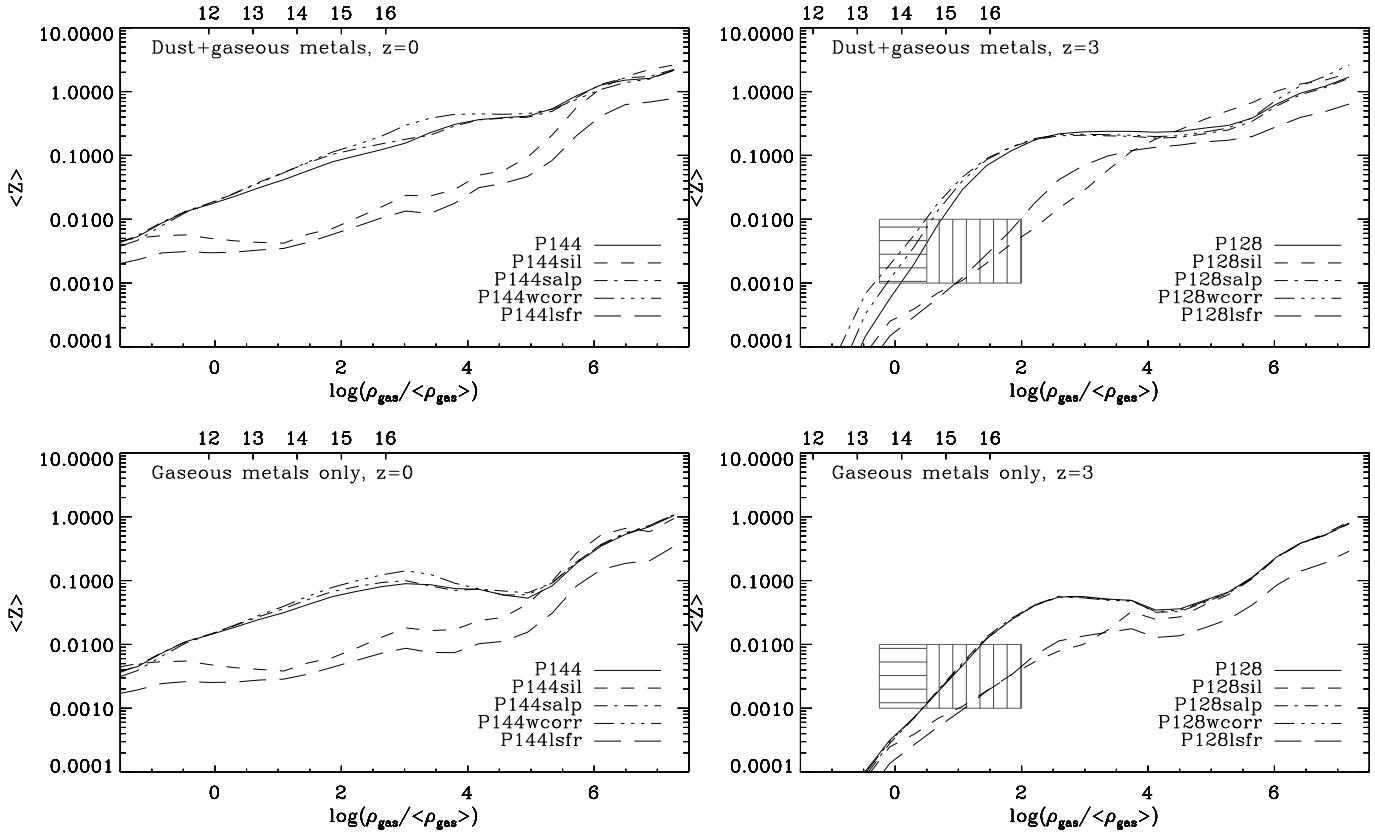

FIG. 12.— Enrichment of the IGM for radiation pressure driven dust ejection, for several models (see Table 8) at $z = 0$ (left panels) and at $z = 3$ (right panels). Plotted quantities are as in the top panel of Fig 2. Top panels show total (gas+dust) abundances and bottom panels show only gas phase abundances (after thermal sputtering).

cant fraction of cluster metals. It also fits the stellar M-Z relation reasonably well at intermediate masses, but not at high masses (where none of our models predict high enough metallicity).

Dust can be ejected from galaxies by radiation pressure if three basic conditions hold. First, the luminosity/mass ratio toward the galaxy must be large enough that radiation pressure exceeds the gravitational force. Second, the gas drag on dust must be small enough that dust can pass through the dense gaseous part of the galaxy and into the halo/IGM before being destroyed. Third, the dust must not be confined by magnetic fields that are bound to the gas. In this study, we have addressed only the first condition, distributing the dust at the radius where gravitational and radiation pressure forces balance. We have *not* addressed whether dust can truly decouple from the gas or, if so, what dust outflow rate ensues.

The trials presented in this section indicate that with reasonable assumptions about the grain properties, spectral synthesis and dust correction and with neglect of extra light from quasars and extra force on grains from the photoelectric effect – each of which gives approximately a factor of two uncertainty in the radiation pressure force – a significant fraction of the dust can be expelled from the simulated galaxies. This conclusion would change only if several of the uncertainties conspired to make the force an order of magnitude or more smaller than we have estimated.

The main weakness of our method is a poor understanding of dust ejection itself, and in particular how well magnetic fields can confine grains to galaxies. Assuming that grains can escape, our method can provide strong predictions of the spatial distribution, grain-size distribution and destruction of dust, as well as the extinction and reddening due to IG dust. These predictions will be presented in detail in a future study.

8. CONCLUSIONS

We have developed a new method of calculating the chemical evolution of galaxies and of the IGM, with particular emphasis on the physical mechanisms that remove metals from galaxies. The method is applied to already-completed cosmological simulations, so it can be run quickly to test changes in the assumed prescriptions and parameters. In the method, metals are instantaneously placed in gas that is in and nearby galaxies, according to parameterized physical prescriptions that estimate where the metals would 'land' in the gas after $\sim 10^8 - 10^9\,\mathrm{yr}$. We have discussed in detail the prescriptions used in this study, pointing out which physical effects are captured by them. The method can be used to predict the cosmological distribution of metals *given* assumptions about their ejection, or conversely to study the ejection assumptions by comparing our calculations to observations in detail.

In this paper we have applied the method to several cosmological simulations. Using these results we can draw some conclusions both about the methodology we have developed, and about metal ejection in the real universe.

In our simulations, removal of metals by purely dynamical processes such as ram-pressure stripping or tidal disruption of galaxies, is relatively ineffective at polluting the IGM. Averaged over their mass function, galaxies of mass $\gtrsim 10^{10.5}\,\mathrm{M}_\odot$ (i.e. those resolved by our 144^3 particle simulation) lose $\sim 4\%$ of their metals by $z = 0$. This accounts for only about 1/12th of the metal density observed in the gas of rich clusters, though we cannot address the dynamical enrichment of clusters by smaller galaxies that could have comprised a significant fraction of the mass function at high z. Dynamical removal alone also cannot account for the mass-metallicity relation observed in present-day galaxies of all masses. Galaxies of mass $M \gtrsim 10^{8.5}\,\mathrm{M}_\odot$ also lose $\sim 2\%$ of their metals by $z = 3$, enriching Lyα absorbers with $N(H\,I) \sim 10^{14.5}\,\mathrm{cm}^2$ to $\sim 10^{-4.5}\,Z_\odot$, about 100 times less than observed. These results indicate that *if* dynamical removal were to account for metals in the low-density Lyα absorbers (Gnedin & Ostriker 1997; Gnedin 1998), it must have been by smaller galaxies, presumably at very high redshifts ($z \gg 6$). We also find that the dynamical removal of metals is enhanced if the metals are moved into galaxy halos (i.e., by winds or dust-ejection), but only slightly and only at low z; at high z the net effect of dynamics is to move metals from low- to high-density regions.

If the metals in the IGM came from fairly massive galaxies at $z \lesssim 6$, some mechanism other than dynamical removal must have played an important role. Supernova-driven winds are a plausible candidate. Our prescription assumes that winds develop at a critical SFR/area, with a fixed velocity, and an energy in the wind proportional to the SFR. We find that the degree of IGM enrichment is not very sensitive to the wind efficiency (unless it is very different than we have assumed) or how the metals are distributed within the wind 'stopping radius'. The results *are* sensitive to the assumed fraction of the ambient material entrained by the wind, the wind outflow velocity, and the critical SFR. If the latter is chosen so that a significant fraction of high-z galaxies drive winds (as indicated by observations of Lyman-break galaxies; see Steidel et al. 2000 and Pettini et al. 2001), then winds with outflow velocities of $\sim 200\,\mathrm{km\,s}^{-1}$ or more (as also indicated by the observations) can escape to large distances, and enrich the low-density IGM to roughly the level observed at $z \sim 3$. Whether the enrichment can match the observed metallicities in detail, and whether the wind process itself would disturb the low-density IGM more than allowed by observations is an important and open question (see Theuns, Mo & Schaye [2001] for some discussion of the latter).

At lower redshifts, winds even from massive galaxies may be important, though in our models metal ejection from galaxies of $M \gtrsim 10^{10.5}\,\mathrm{M}_\odot$ probably cannot account for all of the metals in cluster gas unless a rather extreme model is adopted or one of our methodological assumptions is changed. Since smaller galaxies eject metals more efficiently, it is possible that winds could account for the ICM metallicity if these were included. Wind ejection also leads to a mass-metallicity relation comparable to – but somewhat steeper than – that observed. Using future simulations with a larger range of galaxy masses, the M-Z relation should be a useful diagnostic of outflows, as it helps break the degeneracy between our model parameters in determining the metal ejection efficiency.

The ejection of dust by radiation pressure is another interesting way that metals may escape galaxies. We assume that a significant fraction of galactic dust escapes to the radius where gravitational and radiation-pressure forces balance. We find that our basic results are not strongly

TABLE 8
RADIATION PRESSURE MODELS RUN

Model	Variation	$f_{\rm IGM}$	$\langle Z_{\delta=1}\rangle$	$\langle Z_{\delta=100}\rangle$	$\langle Z_{\rm cl}\rangle$	$\langle Z_{\rm gal}\rangle$	C_f
P144	none	0.16	0.018	0.087	0.19	0.71	-0.96
P64	64^3 run	0.32	0.00072	0.08	-	0.39	-0.96
P128	128^3 run	0.27	0.00089	0.14	-	0.48	-0.96
P144salp	Salpeter IMF	0.19	0.019	0.11	0.20	0.68	-0.81
P128salp	SALP, 128^3	0.33	0.0028	0.15	-	0.45	-0.81
P144sil	silicate grains	0.04	0.005	0.0084	0.03	0.86	-1.05
P128sil	SIL, 128^3	0.033	0.00028	0.0055	-	0.65	-1.05
P144lsfr	$\epsilon_* = 0.355$	0.061	0.003	0.0065	0.021	0.30	-0.33
P128lsfr	$\epsilon_* = 0.355$, 128^3	0.098	0.00018	0.012	-	0.20	-0.33
P144scorr	$F_{\rm FIR}/F_{\rm opt} = 2$	0.11	0.015	0.052	0.12	0.77	-0.64
P128scorr	sCORR, 128^3	0.24	0.00064	0.12	-	0.50	-0.64
P144wcorr	$F_{\rm FIR}/F_{\rm opt} = 1/3$	0.20	0.019	0.11	0.22	0.67	-1.26
P128wcorr	$F_{\rm FIR}/F_{\rm opt} = 1/3$	0.29	0.0012	0.15	-	0.47	-1.26
P144lcorr	Luminosity correction	0.15	0.016	0.073	0.16	0.73	-1.09
P128lcorr	Luminosity correction	0.28	0.0011	0.14	-	0.48	-1.09
P144ccorr	const. correction	0.15	0.016	0.077	0.18	0.73	0
P128ccorr	const. correction	0.22	0.00054	0.12	-	0.51	0

Note: all results are given at $z = 0$ for the 144^3 run, and at $z = 3$ for the other two runs.

sensitive to the assumed IMF or dust correction. The results do, however, depend on the grain type and on the very important assumption that the grains are not confined by the gas or magnetic fields in galaxies. The results show that metals removed from $\gtrsim 10^{8.5}\,{\rm M}_\odot$ galaxies as dust, then destroyed in the IGM or galaxy halos by sputtering, could also account for the mean level of IGM enrichment observed at $z = 3$ – although again it is unclear whether the distribution agrees with the observations in detail. At low redshift, massive galaxies can enrich the ICM to the observed levels. Moreover, since dust ejection does not 'avoid' high-pressure regions as winds do, dust can enrich intragroup gas more uniformly than winds. Enrichment of the IGM by dust would provide a number of chemical signatures; in particular, non-depleted elements such at N and Zn should be underrepresented in the IGM (see Aguirre et al. 2001b).

Most generally, our simulations support the view that a significant fraction of cosmic metals lie in the IGM, and our method provides a useful way to generate predictions of the cosmic distribution of metals usable in a number of ways. With higher-resolution simulations we should be able to more effectively test the importance of low mass galaxies at all redshifts, as well as perform more careful resolution tests of our results. Future observations, as well as more detailed small-scale simulations, will help to develop more accurate ejection prescriptions.

This work was supported by NASA Astrophysical Theory Grants NAG5-3922, NAG5-3820, and NAG5-3111, by NASA Long-Term Space Astrophysics Grant NAG5-3525, and by the NSF under grants ASC93-18185, ACI96-19019, and AST-9802568. JG was supported by NASA Grant NGT5-50078 for the duration of this work, and AA was supported in part by the National Science Foundation grant no. PHY-9507695 and by a grant in aid from the W.M. Keck Foundation. The simulations were performed at the San Diego Supercomputer Center, and the post-simulation processing used a computer purchased under the National Science Foundation grant no. PHY-9507695.

REFERENCES

Abadi, M. G., Moore, B. & Bower, R. G. 1999, MNRAS, 308, 947
Abel, T., Anninos, P., Norman, M. L. & Zhang, Y. 1998, ApJ, 508, 518
Aguirre, A., Hernquist, L., Weinberg, D., Katz, N., & Gardner, J. 2001a. ApJ, in press; astro-ph/0006345
Aguirre, A., Hernquist, L., Katz, N., Gardner, J., & Weinberg, D. 2001b. ApJ, in press; astro-ph/0006346
Aguirre, A. 1999, ApJ, 525, 583
Balsara, D., Livio, M., & O'Dea, C. P. 1994, ApJ, 437, 83
Barnes, J. E. 1988, ApJ, 331, 699
Barnes, J. E. & Hernquist, L. 1992, ARA&A, 30, 705
Breitschwerdt, D., Voelk, H. J. & McKenzie, J. F. 1991, A&A, 245, 79
Breitschwerdt, D. & Schmutzler, T. 1999, A&A, 347, 650
Bruzual, A. G., & Charlot, S. 1993, ApJ, 405, 538
Buote, D. A. 2000, MNRAS, 311, 176
Carr, B. J., Bond, J. R. & Arnett, W. D. 1984, ApJ, 277, 445
Calzetti, D. & Heckman, T. M. 1999, ApJ, 519, 27
Cen, R., Miralda-Escudé, J., Ostriker, J. P. & Rauch, M. 1994, ApJ, 427, L9
Cen, R. & Ostriker, J. P. 1999, ApJ, 519, L109
Chiao, R. Y. & Wickramasinghe, N. C. 1972, MNRAS, 159, 361
Cowie, L. L., Songaila, A., Kim, T., & Hu, E. M. 1995, AJ, 109, 1522
Cowie, L. L. & Songaila, A. 1998, Nature, 394, 44
Davé, R., Hellsten, U., Hernquist, L., Katz, N. and Weinberg, D. H. 1998, ApJ, 509, 661
Davé, R., Hernquist, L., Katz, N., & Weinberg, D. 1999a, ApJ, 511, 521

Davé, R., Gardner, J. P., Hernquist, L., Katz, N., & Weinberg, D. 1999b, to appear in The Evolution of Galaxies on Cosmological Timescales, eds. J. E. Beckman and T. J. Mahoney, ASP books (1999); astro-ph/9910220
David, L. P., Forman, W. & Jones, C. 1990, ApJ, 359, 29
David, L. P., Forman, W. & Jones, C. 1991, ApJ, 380, 39
Davies, J. I., Alton, P., Bianchi, S. & Trewhella, M. 1998, MNRAS, 300, 1006
Davis, D. S., Mulchaey, J. S. & Mushotzky, R. F. 1999, ApJ, 511, 34
Dekel, A. & Silk, J. 1986, ApJ, 303, 39
Duley, W. W., Jones, A. P. & Williams, D. A. 1989, MNRAS, 236, 709
Efstathiou, G. 2000, MNRAS, 317, 697
Ellison, S. L., Songaila, A., Schaye, J. & Pettini, M. 2000, AJ, 120, 1175
Ferrara, A., Aiello, S., Ferrini, F. & Barsella, B. 1990, A&A, 240, 259
Ferrara, A., Pettini, M., & Shchekinov, Y. 2000, MNRAS, 319, 539
Ferrara, A. & Tolstoy, E. 2000, MNRAS, 313, 291
Finoguenov, A., David, L. P., & Ponman, T. J. 2000, ApJ, 544, 188
Folkes, S. et al. 1999, MNRAS, 308, 459
Fukugita, M., Hogan, C. J. & Peebles, P. J. E. 1998, ApJ, 503, 518
Fukumoto, J. & Ikeuchi, S. 1996, PASJ, 48, 1
Gavazzi, G., Pierini, D. & Boselli, A. 1996, A&A, 312, 397
Gnedin, N. Y. & Ostriker, J. P. 1997, ApJ, 486, 581
Gnedin, N. Y. 1998, MNRAS, 294, 407
Gould, A. , Flynn, C. & Bahcall, J. N. 1998, ApJ, 503, 798
Granato, G. L., Lacey, C. G., Silva, L., Bressan, A., Baugh, C. M., Cole, S., & Frenk, C. S. 2000, ApJ, 542, 710
Gunn, J. E. & Gott, J. R. I. 1972, ApJ, 176, 1
Haardt, F. & Madau, P. 1996, ApJ, 461, 20
Haiman, Z. & Loeb, A. 1997, ApJ, 483, 21
Heckman, T.M. 2000, astro-ph/0009075
Heckman, T. M., Robert, C. , Leitherer, C. , Garnett, D. R. & van der Rydt, F. 1998, ApJ, 503, 646
Heckman, T. M., Lehnert, M. D., Strickland, D. K., & Armus, L. 2000, ApJS, 129, 493 [HLSA]
Heckman, T. M., Armus, L. & Miley, G. K. 1990, ApJS, 74, 833
Hellsten, U., Dave, R., Hernquist, L., Weinberg, D. H., & Katz, N. 1997, ApJ, 487, 482
Hellsten, U., Hernquist, L., Katz, N. & Weinberg, D. H. 1998, ApJ, 499, 172
Hernquist, L. 1992, ApJ, 400, 460
Hernquist, L. 1993, ApJ, 409, 548
Hernquist, L., Katz, N., Weinberg, D.H. & Miralda-Escudé, J. 1996, ApJ, 457, L51
Hernquist, L. & Katz, N. 1989, ApJS, 70, 419
Impey, C, & Bothun, G. 1997, ARA&A, 35, 267.
Jones, A. P., Tielens, A. G. G. M., Hollenbach, D. J. & McKee, C. F. 1994, ApJ, 433, 797
Katz, N. , Weinberg, D. H. & Hernquist, L. 1996, ApJS, 105, 19
Kennicutt, R. C. 1998, ApJ, 498, 541
Kim, S. -H. , Martin, P. G. & Hendry, P. D. 1994, ApJ, 422, 164
Kobayashi, C. & Arimoto, N. 1999, ApJ, 527, 573
Laor, A. & Draine, B. T. 1993, ApJ, 402, 441
Lehnert, M. D. & Heckman, T. M. 1996, ApJ, 462, 651
Lehnert, M. D., Heckman, T. M. & Weaver, K. A. 1999, ApJ, 523, 575
Mac Low, M. -M. & Ferrara, A. 1999, ApJ, 513, 142
Madau, P., Ferrara, A., & Rees, M. 2000, ApJ, submitted; astro-ph/0010158
Madau, P. & Pozzetti, L. 2000, MNRAS, 312, L9
Martin, C. L. 1999, ApJ, 513, 156
Mathis, J. S. & Whiffen, G. 1989, ApJ, 341, 808
Metzler, C. A. & Evrard, A. E. 1994, ApJ, 437, 564
Metzler, C. A. & Evrard, A. E. 1997, ApJ, submitted; astro-ph/9710324
Murakami, I. & Babul, A. 1999, MNRAS, 309, 161
Murali, C., Katz, N., Hernquist, L., Weinberg, D., & Davé, R. 2001, ApJ, submitted; astro-ph/0106282
Mushotzky, R., Loewenstein, M., Arnaud, K. A., Tamura, T., Fukazawa, Y., Matsushita, K., Kikuchi, K. & Hatsukade, I. 1996, ApJ, 466, 686
Nath, B. B. & Chiba, M. 1995, ApJ, 454, 604
Nath, B. B. & Trentham, N. 1997, MNRAS, 291, 505
Ostriker, J. P. & Gnedin, N. Y. 1996, ApJ, 472, L63
Pagel, B. E. J. 1997, Nucleosynthesis and Chemical Evolution of Galaxies (Cambridge: Cambridge University press)
Pagel, B. 1999, invited review, Ringberg Workshop: 'Galaxies in the Young Universe II', Aug. 2–6 1999, Hans Hippelein (ed.), Springer-Verlag; astro-ph/9911204
Pearce, F. R., Jenkins, A., Frenk, C. S., Colberg, J. M., White, S. D. M., Thomas, P. A., Couchman, H. M. P., Peacock, J. A., & Efstathiou, G. 1999, ApJ, 521, L99
Pei, Y. C., Fall, S. M. & Hauser, M. G. 1999, ApJ, 522, 604
Persic, M. & Salucci, P. 1997, ASP Conf. Ser. 117: Dark and Visible Matter in Galaxies and Cosmological Implications.
Pettini, M., Ellison, S. L., Steidel, C. C. & Bowen, D. V. 1999, ApJ, 510, 576
Pettini, M. , Steidel, C. C., Adelberger, K. L., Dickinson, M. & Giavalisco, M. 2000, ApJ, 528, 96
Pettini, M. , King, D. L., Smith, L. J. & Hunstead, R. W. 1997, ApJ, 478, 536
Pettini, M., Shapley, A., Steidel, C. C., Cuby, J.-G., Dickinson, M., Moorwood, A.F.M., Adelberger, K. L., Dickinson, M., & Giavalisco, M. 2001, ApJ, in press; astro-ph/0102456
Prochaska, J. X. & Wolfe, A. M. 2000, ApJ, 533, L5
Quilis, V., Moore, B., & Bower, R. 2000, Science, 288, 1617
Rauch, M., Haehnelt, M. G. & Steinmetz, M. 1997, ApJ, 481, 601
Renzini, A. , Ciotti, L. , D'Ercole, A. & Pellegrini, S. 1993, ApJ, 419, 52
Renzini, A. 1997, ApJ, 488, 35
Renzini, A. 1999, to appear in "Chemical Evolution from Zero to High Redshift", ed. by J. Walsh & M. Rosa (Berlin: Springer); astro-ph/9902361
Renzini, A. 2000, to appear in "Large Scale Structure in the X-Ray Universe", ed. I. Georgantopoulos & M. Plionis (Gyf sur Yvette, Ed. Frontieres); astro-ph/0001312
Salucci, P. & Persic, M. 1999, MNRAS, 309, 923
Scalo, J. M. 1986, Fundamentals of Cosmic Physics, 11, 1
Scannapieco, E. & Broadhurst, T. 2001, ApJ, 549, 28
Schaye, J., Rauch, M., Sargent, W. L. W., & Kim, T. 2000, ApJ, 541, L1
Shustov, B. M. & Vibe, D. Z. 1995, Astronomy Reports, 39, 578
Simonsen, J. T. & Hannestad, S. 1999, A&A, 351, 1
Songaila, A. 1997, ApJ, 490, L1
Songaila, A. & Cowie, L. L. 1996, AJ, 112, 335
Steidel, C. C., Adelberger, K. L., Giavalisco, M., Dickinson, M. & Pettini, M. 1999, ApJ, 519, 1
Steidel, C. C., Adelberger, K. L., Shapley, A. E., Pettini, M., Dickinson, M. & Giavalisco, M. 2000, ApJ, 532, 170
Strickland, D. K. & Stevens, I. R. 2000, MNRAS, 314, 511
Tegmark, M., Silk, J., & Evrard, A. 1993, ApJ, 417, 54
Tegmark, M., Silk, J., Rees, M. J., Blanchard, A., Abel, T. & Palla, F. 1997, ApJ, 474, 1
Theuns, T., Mo, H. J., & Schaye, J. 2001, MNRAS, 321, 450
Wang, B. & Heckman, T. M. 1996, ApJ, 457, 645
Weinberg, D.H., Davé, R., Gardner, J.P., Hernquist, L., & Katz, N. 1999, in "Photometric Redshifts and High Redshift Galaxies", eds. R. Weymann, L. Storrie-Lombardi, M. Sawicki & R. Brunner, (San Francisco: ASP Conference Series), p. 341
Weinberg, D.H., Hernquist, L., & Katz, N. 2000, ApJ, submitted; astro-ph/0005340
Weingartner, J.C., & Draine, B.T. 1999, ApJ, submitted; astro-ph/990725
Weingartner, J.C., & Draine, B.T. 1999, ApJ, submitted; astro-ph/0010117
White, D. A. 2000, MNRAS, 312, 663
Zaritsky, D. , Kennicutt, R. C. , Jr. & Huchra, J. P. 1994, ApJ, 420, 87
Zhang, Y., Anninos, P., & Norman, M.L. 1995, ApJ, 453, L57
Zucca, E. et al. 1997, A&A, 326, 477